The Cryosphere
Discussions

Open Access

EGU

1 # Reconstruction of the Greenland Ice Sheet surface

2 # mass balance and the spatiotemporal distribution of

3 # freshwater runoff from Greenland to surrounding seas

4 SEBASTIAN H. MERNILD

5 *Nansen Environmental and Remote Sensing Center, Bergen, NORWAY, Direction of Antarctic*
6 *and Sub-Antarctic Programs, Universidad de Magallanes, Punta Arenas, CHILE, and Faculty of*
7 *Engineering and Science, Western Norway University of Applied Sciences, Sogndal, NORWAY*
8

9 GLEN E. LISTON

10 *Cooperative Institute for Research in the Atmosphere, Colorado State University, Fort Collins,*
11 *Colorado, USA*
12

13 ANDREW P. BECKERMAN

14 *Department of Animal and Plant Sciences, University of Sheffield, UK*

15

16 JACOB C. YDE

17 *Faculty of Engineering and Science, Western Norway University of Applied Sciences, Sogndal,*
18 *NORWAY*
19

20

21

22

23

24 **Corresponding author address:**

25 Sebastian H. Mernild, e-mail: sebastian.mernild@nersc.no

The Cryosphere
Discussions

Open Access

EGU

Abstract

Knowledge about variations in runoff from Greenland to adjacent fjords and seas is important for the hydrochemistry and ocean research communities to understand the link between terrestrial and marine Arctic environments. Here, we simulate the Greenland Ice Sheet (GrIS) surface mass balance (SMB), including refreezing and retention, and runoff together with catchment-scale runoff from the entire Greenland landmass ($n = 3,272$ simulated catchments) throughout the 35-year period 1979–2014. SnowModel/HydroFlow was applied at 3-h intervals to resolve the diurnal cycle and at 5-km horizontal grid increments using ERA-Interim (ERA-I) reanalysis atmospheric forcing. Simulated SMB was low compared to earlier studies, whereas the GrIS surface conditions and precipitation were similar. Variations in meteorological and surface ice and snow cover conditions influenced the seasonal variability in simulated catchment runoff; variations in the GrIS internal drainage system were assumed negligible and a time-invariant digital elevation model was applied. Approximately 80 % of all catchments showed increasing runoff trends over the 35 years, with on average relatively high and low catchment-scale runoff from the SW and N parts of Greenland, respectively. Outputs from an Empirical Orthogonal Function (EOF) analysis were combined with cross-correlations indicating a direct link (zero lag time) between modeled catchment-scale runoff and variations in the large-scale atmospheric circulation indices North Atlantic Oscillation (NAO) and Atlantic Multidecadal Oscillation (AMO). This suggests that natural variabilities in AMO and NAO constitute major controls on catchment-scale runoff variations in Greenland.

KEYWORDS: Empirical Orthogonal Function; Greenland freshwater runoff; Greenland Ice Sheet; HydroFlow; Modeling; NASA MERRA; SnowModel; surface mass-balance

1. Introduction

The Greenland Ice Sheet (GrIS) is highly sensitive to changes in climate (e.g., Box et al.
2012; Hanna et al. 2013; Langen et al. 2015; Wilton et al. 2016; AMAP 2017). It is of scientific
interest and importance because it constitutes a massive reserve of freshwater that discharges to
adjacent fjords and seas (Cullather et al. 2016). Runoff from Greenland influences the sea
surface temperature, salinity, stratification, marine ecology, and sea-level in a number of direct
and indirect ways (e.g., Rahmstorf et al. 2005; Straneo et al. 2011; Shepherd et. al. 2012; Weijer
et al. 2012; Church et al. 2013; Lenaerts et al. 2015).

The GrIS surface mass balance (SMB) and freshwater runoff have changed over the last
decades and most significantly since the mid-1990s (e.g., Church et al. 2013; Wilton et al. 2016).
For example, recent estimates by Wilton et al. (2016) showed a decrease in SMB from ~350 Gt
yr^{-1} (early-1990s) to ~100 Gt yr^{-1} (late-2000s) and an increase in runoff from ~200 Gt yr^{-1} (early-
1990s) to ~450 Gt yr^{-1} (late-2000s). For 2009 through 2012, the runoff has been estimated to
include approximately two-third of the gross GrIS mass loss (Enderlin et al. 2014), while the net
GrIS mass loss, on average, was 375 Gt yr^{-1} (2011–2014) (AMAP 2017). The contribution of
GrIS mass loss to global mean sea-level was around 5 % in 1993, and more than 25 % in 2014
(Chen et al. 2017). Noël et al. (2017), however, estimated the GrIS and peripheral glaciers to
contribute approximately 43 % to the contemporary sea-level rise.

Runoff from the GrIS is an integrated response of rain, snowmelt, and glacier melt and
other hydrometeorological processes (e.g., Bliss et al. 2014). Tedesco et al. (2016) estimated a
1979–2016 change in GrIS spatial surface melt extent of ~15,820 km^2 yr^{-1}, and a change in
surface ablation duration of ~30–40 days in NE and 15–20 days along the west coast. At higher
GrIS elevations, surface melt does not necessarily equal surface runoff because meltwater may

72   refreeze in the porous near-surface snow and firn layers (Machguth et al. 2016) where the firn

73   pore space provides potential storage for meltwater (Haper et al. 2012; van Angelen et al. 2013).

74   Melt water percolation, refreezing, and densification processes are common in GrIS snow, firn,

75   and multi-year firn layers – especially where semipermeable or impermeable ice layers are

76   present (Brown et al. 2012; van As et al. 2016). Such physical mechanisms and conditions in the

77   firn and multi-year firn layers lead, e.g., to non-linearity in meltwater retention (Brown et al. 2012).

78   The GrIS internal drainage system has received increased attention in recent years. This

79   is, in part, because the summer acceleration of ice flow is controlled by supraglacial meltwater

80   draining to the subglacial environment (Zwally et al. 2002; van de Wal et al. 2008; Shephard et

81   al. 2009). Enhanced production of supraglacial meltwater results in more water supplied to the

82   glacier bed, leading to reduced basal drag and accelerated basal ice motion. This process is

83   referred to as basal lubrication, and it constitutes a potential positive feedback mechanism

84   between climate change and sea-level rise (Hewitt 2013). At high GrIS elevations, surface

85   meltwater primarily drains to the glacier bed via hydrofractures (van der Veen 2007), whereas

86   meltwater is routed to the glacier bed via crevasses and moulins in the peripheral areas (Banwell

87   et al. 2016; Everett et al. 2016; Koziol et al. 2017). Rapid drainage of large volumes of GrIS

88   meltwater come from sudden release from supraglacial and proglacial lakes (known as a glacial

89   lake outburst flood (GLOF) or jökulhlaup), which are particular common in West Greenland

90   (Selmes et al. 2011; Carrivick and Quincey 2014). The seasonal evolution of the structure and

91   efficiency of the drainage system beneath the GrIS is indirectly assumed from our understanding

92   of the subglacial hydraulic potential beneath Alpine glaciers. This general understanding is used

93   explain the observed seasonal changes in ice motion (Bartholomew et al. 2010, 2012) where few

94   direct observations exist (Kohler et al. 2017). In fact, we know very little about spatiotemporal

95   shifts in the configuration of the subglacial drainage network beneath the GrIS. We therefore

96   assume that the subglacial drainage network in the natural system is dynamic and sensitive to

97   rerouting of water flow between adjacent catchments (so-called water piracy; Chu et al. 2016),

98   although we do not understand the details sufficiently to implement them in a runoff routing

99   model.

100   We also lack high resolution information on the spatiotemporal distribution of GrIS and

101   Greenland freshwater runoff to the fjords and seas, and the spatiotemporal distribution of solid-

102   ice discharge (calving) from tidewater glaciers is also largely unknown (Howat et al. 2013). To

103   address this lack of knowledge, information about the quantitative discharge (runoff and solid-

104   ice discharge) conditions from the numerous of catchments in Greenland is required. Available

105   GrIS calving rates are insufficient to represent the calving rates from the entire Greenland and

106   are therefore not generally included in overall Greenland freshwater estimates (Nick et al. 2009;

107   Lenaerts et al. 2015). This is an unaddressed gap, which likely prevents us from

108   comprehensively understanding the terrestrial freshwater discharge to the fjords and seas. This

109   also limits the subsequent the link between changes in terrestrial inputs and changes in the

110   hydrographic and circulation conditions. This unaddressed knowledge gap has further

111   implications for ocean model simulations, where, for example, earlier representations of

112   Greenland discharge boundary conditions were either non-existent or overly simplistic (e.g.,

113   Weijer et al. 2012).

114   Previous GrIS studies constructed a section-wise runoff distribution by dividing the ice

115   sheet into six to eight overall defined sections (e.g., Rignot et al. 2008; Bamber et al. 2012;

116   Rignot and Mouginot 2012; Lenaerts et al. 2015; Wilton et al. 2016). These studies illustrated an

The Cryosphere
Discussions

Open Access

EGU

117   increase in runoff since 1870 for all GrIS sections, with the greatest increase in runoff since mid-

118   1990s and in the SW part of the ice sheet.

119   Mernild and Liston (2012) reconstructed the GrIS SMB and the Greenland

120   spatiotemporal runoff distribution from ~3,150 individually simulated catchments, at 5-km

121   spatial, and daily temporal, resolutions covering the period from 1960 through 2010. Automatic

122   weather stations located both on and off the GrIS were used for atmospheric forcings, and the

123   study was carried out using a full energy balance, multi-layer snowpack and snow distribution,

124   and freshwater runoff model and software package called SnowModel/HydroFlow (Liston and

125   Elder 2006a; Liston and Mernild 2012). These individual catchment outlet runoff time series

126   were analyzed to map runoff magnitudes and variabilities in time, but also emphasized trends

127   and spatiotemporal variations, including runoff contributions from the GrIS, the land area

128   between the GrIS ice margin and the ocean, from the relatively small isolated glaciers and ice

129   caps, and from entire Greenland. This approach is especially important when trying to

130   understand the total runoff fraction from Greenland, including the annual and seasonal

131   freshwater runoff variabilities within individual catchments.

132   Here, we improve the work by Mernild and Liston (2012) by using an updated version of

133   SnowModel/HydroFlow and by including a new digital elevation model (DEM). We also extend

134   the time series to 2014 by using the ERA-Interim (ERA-I) reanalysis products on 3-h time step

135   (Dee et al. 2011). The objective of this study is to simulate, map, and analyze first-order

136   atmospheric forcings and GrIS mass balance components for Greenland. The analyzed variables

137   include the GrIS SMB, together with GrIS surface air temperature, surface melt, precipitation,

138   evaporation, sublimation, refreezing and retention, and surface freshwater runoff and specific

139   runoff (runoff volume per time per unit drainage area, $L\ s^{-1}\ km^{-2}$; to convert to $mm\ yr^{-1}$, multiply

The Cryosphere
Discussions

140   by 31.6) conditions. The time period covers 1979–2014 (35 years), with a focus on the present

141   day conditions 2005–2014 (the last decade of the simulations). Further, the spatiotemporal

142   magnitude, distribution, and trends of individual catchment-scale runoff and specific runoff from

143   Greenland ($n = 3,272$; where n is the number of simulated catchments, each with an individual

144   flow network) were simulated based on HydroFlow-generated watershed divides and flow

145   networks for each catchment. The simulated spatiotemporal catchment-scale outlet runoff is

146   useful as boundary conditions for fjord and ocean model simulations. We also analyzed the

147   spatiotemporal catchment-scale outlet runoff using Empirical Orthogonal Functions (EOF). This

148   analysis allowed us to describe simultaneously how the spatial patterns of catchment-scale outlet

149   runoff changed over time. It also allowed us to explore via cross-correlations the relationship

150   between the spatiotemporal patterns and large-scale atmospheric-ocean circulation indices

151   including the North Atlantic Oscillation (NAO) and the Atlantic Multidecadal Oscillation

152   (AMO), with particular attention to the lag-times, if any, between variations in NAO and AMO

153   and responses in Greenland catchment-scale runoff.

154

155   **2. Model description, setup, and verification**

156   *2.1 SnowModel*

157   SnowModel (Liston and Elder 2006a) is established by six sub-models, where five of the

158   models were used here to quantify spatiotemporal variations in atmospheric forcing, surface

159   snow properties, GrIS SMB, and Greenland catchment runoff. The sub-model *MicroMet* (Liston

160   and Elder 2006b; Mernild et al. 2006a) downscaled and distributed the spatiotemporal

161   atmospheric fields using the Barnes objective interpolation scheme, where the interpolated fields

162   subsequent were adjusted using known meteorological algorithms, e.g., temperature-elevation,

7

163   wind-topography, humidity-cloudiness, and radiation-cloud-topography relationships (Liston and

164   Elder 2006b). *Enbal* (Liston 1995; Liston et al. 1999) simulated a full surface energy balance

165   considering the influence of cloud cover, sun angle, topographic slope, and aspect on incoming

166   solar radiation, and moisture exchanges, e.g., multilayer heat- and mass-transfer processes within

167   the snow (Liston and Mernild 2012). *SnowTran-3D* (Liston and Sturm 1998, 2002; Liston et al.

168   2007) accounted for the snow (re)distribution by wind. *SnowPack-ML* (Liston and Mernild 2012)

169   simulated multilayer snow depths, temperatures, and water-equivalent evolutions. *HydroFlow*

170   (Liston and Mernild 2012) simulated watershed divides, routing network, flow residence-time,

171   and runoff routing (configurations based on the hypothetical gridded topography and ocean-mask

172   datasets), and discharge hydrographs for each grid cell including from catchment outlets. These

173   sub-models have been tested against independent observations with success in Greenland, Arctic,

174   high mountain regions, and on the Antarctic Ice Sheet with acceptable results (e.g., Hiemstra et

175   al. 2006; Liston and Hiemstra 2011; Beamer et al. 2016). For detailed information regarding the

176   use of SnowModel for the GrIS' or local Greenlandic glaciers' SMB and runoff simulations, we

177   refer to Mernild and Liston (2010, 2012) and Mernild et al. (2010a, 2014).

178

179   *2.2 Meteorological forcing, model configuration and model limitations*

180   SnowModel was forced with ERA-Interim (ERA-I) reanalysis products on a $0.75°$

181   longitude $\times 0.75°$ latitude grid from the European Centre for Medium-Range Weather Forecasts

182   (ECMWF; Dee et al. 2011). The simulations were conducted from 1 September 1979 through 31

183   August 2014 (35 years) (henceforth 1979–2014), where the 6-hour (precipitation at 12-hour)

184   temporal resolution ERA-I data was downscaled to 3-hourly values and a 5-km grid using

185   MicroMet. The 3-hour temporal resolution was chosen to allow SnowModel to resolve the solar

186   radiation diurnal cycle in its simulation of snow and ice temperature evolution and melt

187   processes.

188   The DEM was obtained from Levinsen et al. (2015), and rescaled to a 5-km horizontal

189   grid increment that covered the GrIS (1,646,175 km^2), mountain glaciers, and the entire

190   Greenland (2,166,725 km^2) and the surrounding fjords and seas (Figure 1a). The DEM is time-

191   invariant specific to the year 2010. The DEM was developed by merging contemporary radar and

192   laser altimetry data, where radar data were acquired with Envisat and CryoSat-2, and laser data

193   with the Ice, Cloud, and land Elevation Satellite (ICESat), the Airborne Topographic Mapper

194   (ATM), and the Land, Vegetation, and Ice Sensor (LVIS). Radar data were corrected for

195   horizontal, slope-induced, and vertical errors from penetration of the echoes into the subsurface

196   (Levinsen et al. 2015). Since laser data are not subject to such errors, merging radar and laser

197   data yields a DEM that resolves both surface depressions and topographic features at higher

198   altitudes (Levinsen et al. 2015). The distribution of glacier cover was obtained from the

199   Randolph Glacier Inventory (RGI, v. 5.0) polygons; these data were resampled to the 5-km grid.

200   The SnowModel land-cover mask defined glaciers to be present when individual grid cells were

201   covered by 50 % or more of glacier ice.

202   First, the GrIS DEM was initially divided into six major sections following Rignot et al.

203   (unpublished): southwest (SW), west (W), northwest (NW), north (N), northeast (NE), and

204   southwest (SW) (Figure 1b and Table 1). Second, HydroFlow divided Greenland into 3,272

205   individual catchments (Figure 1c), each with an eight-compass-direction water-flow network

206   where water is transported through this network via linear reservoirs. Only a single outlet into the

207   seas was allowed for each individual catchment.

208   The mean and median catchment sizes were 680 km^2 and 75 km^2, respectively. The top

209   one percent of the largest catchments accounted for 53 % of the Greenland area. This distribution

210   of HydroFlow-defined GrIS catchments (Figure 1c) closely matched both the catchment

211   distribution by Mernild and Liston (2012) and by Rignot and Kanagaratnam (2006) for the 20

212   largest GrIS catchments (not including midsize and minor catchments), both with respect to size

213   and location of the watershed divide. The total number of HydroFlow-generated catchments

214   presented in this study was ~4 % higher than the number of Greenland catchments in the Mernild

215   and Liston (2012) study.

216   In MicroMet, only one-way atmospheric coupling was provided, where the

217   meteorological conditions were prescribed at each time step. In the natural system, the

218   atmospheric conditions would be adjusted in response to changes in surface conditions and

219   properties (Liston and Hiemstra 2011). Due to the use of the 5-km horizontal grid increments,

220   snow transport and blowing-snow sublimation processes (usually produced by SnowTran-3D in

221   SnowModel) were excluded from the simulations because blowing snow does not typically move

222   completely across 5-km distances. Static sublimation was, however, included in the model

223   integrations. In HydroFlow, the generated catchment divides and flow network were controlled

224   by the DEM, i.e., exclusively by the surface topography and not by the development of the

225   glacial drainage system. The role of GrIS bedrock topography on controlling the potentiometric

226   surface and the associated meltwater flow direction was assumed to be a secondary control on

227   discharge processes (Cuffey and Paterson 2010).

228   An example of the HydroFlow generated catchment divides and flow network is

229   illustrated in detail by Mernild et al. (2017; Figure 1c) for the Kangerlussuaq catchment in

230   central West Greenland, which includes a part of the GrIS (67°N, 50°W; SW sector of the GrIS).

231   Because the DEM is time-invariant, no changes though feedbacks from a thinning ice, ice retreat,

232   and from changes in hypsometry will influence the catchment divides and the flow network

233   patterns, including the glacial drainage system. Changes in runoff over time are therefore solely

234   influenced by the climate signal and the surface snow and ice cover conditions (runoff was

235   generated from gridded inputs from rain, snowmelt, and ice melt), not by the glacial drainage

236   system. In HydroFlow, the meltwater flow velocities were gained from dye tracer experiments

237   conducted both through the snowpack (in early and late-summer) and through the englacial and

238   subglacial environments (Mernild et al. 2006b).

239

240   *2.3 Verification*

241   For Greenland, long-term catchment river runoff observations are sparse; at present

242   approximately ten permanent hydrometric monitoring stations are operating, measuring the sub-

243   daily and sub-seasonal runoff variability originating from rain, melting snow, and melting ice

244   from local glaciers and the GrIS. In addition, these observations only span parts of the runoff

245   season, ranging between few weeks to approximately three months. For the Kangerlussuaq area,

246   independent meteorological and snow and ice observational datasets are also available, e.g., K-

247   transect point observed air temperature and SMB and catchment outlet observed discharge (e.g.,

248   van de Wal et al. 2005; van den Broeke et al. 2008a; 2008b, Hasholt et. al. 2013). These

249   observed datasets were used for verification of the SnowModel/HydroFlow ERA-I simulated

250   GrIS mean annual air temperature (MAAT), GrIS SMB, and catchment freshwater runoff

251   presented herein (Mernild et al. 2017). These model verifications showed acceptable results (for

252   further information see Mernild et al. 2017). The use of ERA-I has also showed promising

253   results after a full evaluation estimating changes in ice sheet surface mass balance for the

254   catchments linked to Godthåbsfjord (64° N) in Southwest Greenland (Langen et al. 2015).

255   In the analysis that follows, all correlation trends declared 'significant' are statistically

256   significant at or above the 5 % level ($p<0.05$; based on a linear regression t test).

257

258   *2.4 Surface water balance components*

259   For the GrIS, surface water balance components can be estimated using the hydrological

260   method (continuity equation) (Equation 1):

261

262    $P - (Su + E) - R + \Delta S = 0 \pm \eta,$ (1)

263

264   where P is precipitation input from snow and rain, Su is sublimation from a static surface, E is

265   evaporation, R is runoff from snowmelt, ice melt, and rain, ΔS is change in storage (ΔS is also

266   referred to as SMB) derived as the residual value from changes in glacier and snowpack storage.

267   For snow and ice surfaces, the ablation was estimated as: $Su + E + R$. The amount of snow

268   refreezing and retention was estimated as: $P_{rain} + melt_{surface} - R$ (for bare ice: $P_{rain} + melt_{surface} =$

269   R). The parameter η is the water balance discrepancy. This discrepancy should be 0 (or small), if

270   the components P, Su, E, R, and ΔS have been determined accurately.

271

272   **3. EOF runoff analysis**

273   We applied an Empirical Orthogonal Function (EOF) analysis to define the

274   spatiotemporal pattern in simulated catchment outlet runoff. EOF is a statistical tool that

275   analyzes spatial and temporal runoff data to find combinations of locations that vary consistently

The Cryosphere
Discussions

Open Access

EGU

276   through time, and combinations of time, that vary in a spatially consistent manner (e.g.,

277   Preisendorfer 1998; Sparnocchia et al. 2003). The major axes of the EOF analysis identify

278   variations in the catchment outlet runoff in both time and space.

279   The eigenvalues of the EOFs can be correlated with the temporal data, and the

280   eigenvectors with spatial locations, to identify how the EOF describes change in runoff in time

281   and across space. Furthermore, the temporal patterns embedded in the EOFs can, via cross-

282   correlation analysis, be related to larger scale atmospheric-ocean indices (Mernild et al. 2015), in

283   this case the North Atlantic Oscillation (NAO) and Atlantic Multi-decadal Oscillation (AMO).

284   The NAO and AMO indices were obtained from Hurrell and van Loon (1997) and Kaplan et al.

285   (1998), respectively. This latter analysis can generate hypotheses about whether, for example,

286   NAO or AMO leads by some years changes in mass balance and runoff (the lag in the cross-

287   correlation analyses tells us these details).

288   We focused on the NAO and AMO for several reasons. NAO is estimated based on the

289   mean sea-level pressure difference between the Azores High and Icelandic Low. NAO is a large-

290   scale atmospheric circulation index, and is therefore a good measure of airflow and jet-stream

291   moisture transport variability (e.g., Overland et al. 2012) from the North Atlantic onto Northwest

292   Europe (Dickson et al. 2000; Rogers et al. 2001). According to Hurrell (1995), a positive NAO is

293   associated with cold conditions in Greenland, while a negative NAO corresponds to mild

294   conditions. AMO is a large-scale oceanic circulation index, and an expression of fluctuating

295   mean sea-surface temperatures in the North Atlantic (Kaplan et al. 1998). For example, Arctic

296   land surface air temperatures are highly correlated with the AMO (Chylek et al. 2010), and the

297   overall annual trend in the mean GrIS melt extent correlates with the smoothed trends of the

298   AMO (Mernild et al. 2011). A positive AMO indicates relatively high surface air temperature

13

299   and less precipitation at high latitudes (relatively high net mass balance loss), whereas a negative

300   AMO indicates relatively low surface air temperature and a higher precipitation (relatively low

301   net mass balance loss) (Kaplan et al. 1998).

302

303   **4. Results and discussion**

304   *4.1 GrIS surface water balance conditions*

305   Figure 2 presents the SnowModel ERA-I simulated 35-year mean spatial GrIS surface

306   MAAT, precipitation, surface melt, evaporation and sublimation, ablation, and SMB. Overall, all

307   variables follow the expected spatial patterns. For example, the lowest MAAT occurred at the

308   GrIS interior ($\leq$ -27°C) and highest values were at the margin ($\geq$ 0°C). Also, the lowest annual

309   mean precipitation values were situated in the northern half of the GrIS interior ($\leq$ 0.25 m water

310   equivalent (w.e.)), while peak values occurred in the southeastern part of Greenland ($\geq$ 3.5 m

311   w.e.). The lowest annual mean surface melt values ($\leq$ 0.0625 m w.e.) were present at the upper

312   parts of the GrIS and vice versa at the lowest margin areas ($\geq$ 5.0 m w.e.). The 35-year mean

313   SMB illustrated net loss at the lowest elevations of $\geq$ 4.0 m w.e. and net gain at the highest

314   elevations of between 0 and 0.25 m w.e. The peak net gain of $\geq$ 3.5 m w.e. occurred in Southeast

315   Greenland, which matches what is generally expected from the overall precipitation pattern over

316   the GrIS. The SnowModel ERA-I spatial simulated 35-year mean distributions generally agree

317   with previous studies by Fettweis et al. (2008, 2017), Hanna et al. (2011), and Box (2013),

318   within the different temporal domains covered by these studies.

319   On GrIS section-scale (Table 1), a clear variability between the six sections occurred for

320   the surface mass-balance components (Equation 1) for both the 35-year mean and the last

321   decade. On average, most precipitation fell in the Southeast Greenland sector of 242.6 ± 39.1 Gt

322   yr^{-1} (where, ± equals one standard deviation). This was likely due to the cyclonicity between

323   Iceland and Greenland, which typically sets up a prevailing easterly airflow towards the

324   southeastern coast of Greenland that includes orographic enhancement (Hanna et al. 2006; Bales

325   et al. 2009). The lowest 35-year mean precipitation of 31.1 ± 5.4 Gt yr^{-1} occurred in the dry

326   North Greenland. For the last decade, the mean annual precipitation was 232.4 ± 25.2 Gt yr^{-1} and

327   30.9 ± 5.1 Gt yr^{-1} for Southeast Greenland and North Greenland, respectively. This regional

328   distribution is in accordance with the study on Greenlandic precipitation patterns by Mernild et

329   al. (2015), although their analysis was based on observed precipitation from 2001–2012. Further,

330   in Mernild et al. (2017; Figure 6b), the mean ERA-I grid point precipitation (located closest to

331   the center of the Kangerlussuaq watershed) was tested against Kangerlussuaq SnowModel ERA-

332   I downscaled mean catchment precipitation conditions; this analysis indicated no significant

333   difference between the two datasets.

334   The ratio between rain and snow precipitation varied from <1 % (Northeast section) to 5

335   % (Southwest section), averaging 2 % and indicating that rain only played a minor role in the

336   GrIS precipitation budget (Table 1). For the last decade, the average rainfall-to-snowfall ratio

337   was 3 % for the entire GrIS.

338   For the GrIS, the overall precipitation was 653.9 ± 66.4 Gt yr^{-1} (35 years) and 645.0 ±

339   39.0 Gt yr^{-1} (2005–2014), which is within the lower range of previously reported values

340   (Fettweis et al. 2017; Table 1). For example, in MAR (Modèle Atmosphérique Régional; v.

341   3.5.2) the simulated precipitation was between 747.0–642.0 Gt yr^{-1} (1980–1999; snowfall plus

342   rainfall) forced with a variety of forcings, e.g., ERA-40 (Uppala et al. 2005), ERA-I (Dee et al.

343   2011), JRA-55 (Japanese 55-year Reanalysis; Kobayashi et al. 2015).

344   As shown by Fettweis et al. (2017), precipitation is the parameter with the largest

345   uncertainty due to the spread among the different forcing datasets. Also, systematic observational

346   errors may occur during precipitation monitoring, such as wind-induced undercatch, because of

347   turbulence and wind field deformation from the precipitation gauge, wetting losses, and trace

348   amounts (e.g., Goodison et al. 1989; Metcalfe et al. 1994; Yang et al. 1999; Rasmussen et al.

349   2012). An understanding of precipitation conditions and uncertainties are therefore highly

350   relevant for estimating the energy and moisture balances, surface albedo, GrIS SMB conditions,

351   and, in a broader perspective, the GrIS´s contribution to sea-level changes.

352   Besides precipitation, melt and ablation are other relevant parameters for estimation and

353   understanding GrIS surface conditions, where surface melt (including extent, intensity, and

354   duration) is relevant for SMB conditions. An altered surface melt regime can influence surface

355   albedo, because wet snow absorbs up to three times more incident solar energy than dry snow

356   (Steffen 1995), and the energy and moisture balances. Changes in the amount of meltwater also

357   affect total runoff, ice dynamics, and subglacial lubrication and sliding processes (Hewitt 2013).

358   Surface melt varied on a section-scale, for the 35-year mean, from 57.2 ± 24.1 Gt yr^{-1} in

359   North Greenland to 155.2 ± 48.4 Gt yr^{-1} in Southwest Greenland (Table 1). The average for the

360   entire GrIS was 542.9 ± 175.3 Gt yr^{-1} (Table 1). During the last decade, the surface melt for the

361   GrIS had increased to 713.4 ± 138.6 Gt yr^{-1}, varying from 75.9 ± 26.9 Gt yr^{-1} in Northeast

362   Greenland to 202.4 ± 39.2 Gt yr^{-1} in Southwest Greenland. This is an increase of 31 % for the

363   last decade compared to the entire simulation period, which was likely due to increasing MAAT

364   (assuming an empirical relationship between air temperature (sensible heat) and surface melt

365   rates) throughout the simulation period (Hanna et al. 2012).

366   The GrIS ablation patterns varied as expected between the northern and southern sections

367   from 65.7 ± 22.6 Gt yr^{-1} in the north to 132.9 ± 42.2 Gt yr^{-1} in the south. For the entire GrIS, the

368   mean annual ablation was 530.3 ± 153 Gt yr^{-1} and 687.8 ± 118.8 Gt yr^{-1} for the 35-year period

369   and 2005–2014, respectively. This was equal to an increase of 30 %, which was also reflected in

370   the differences in variability from 83.3 ± 24.7 Gt yr^{-1} in North Greenland to 175.1 ± 35.2 Gt yr^{-1}

371   in Southwest Greenland (Table 1).

372   Runoff is a part of the ablation budget and therefore must be quantified to understand

373   GrIS mass balance changes. Runoff varied from 50.0 ± 22.7 Gt yr^{-1} in North Greenland to 112.6

374   ± 41.8 Gt yr^{-1} in South Greenland, averaging 418.1 ± 151.1 Gt yr^{-1} for the 35-year mean period.

375   For 2005–2014, the mean runoff was 73.7 ± 119.8 Gt yr^{-1}; a 37 % increase (Table 1). This

376   increase confirms the results from previous studies (e.g., Wilton et al. 2016). On a regional-scale,

377   runoff varied from 67.6 ± 25.0 Gt yr^{-1} in North Greenland to 154.4 ± 36.3 Gt yr^{-1} in Southwest

378   Greenland. The simulated section runoff distribution was largely in agreement with trends noted

379   by Lewis and Smith (2009) and Mernild and Liston (2012). The section runoff variability

380   roughly followed the precipitation patterns, where sections with high precipitation equaled low

381   runoff (e.g., in Southeast Greenland) and vice versa (e.g., in Southwest Greenland). More

382   specifically, GrIS snowpack retention and refreezing processes suggest that sections with

383   relatively high surface runoff were synchronous with relatively low end-of-winter snow

384   accumulation because more meltwater was retained in the thicker, colder snowpack, reducing

385   and delaying runoff to the internal glacier drainage system (e.g., Hanna et al. 2008). However, in

386   maritime regions such as Southeast Greenland, high surface runoff can result from abnormally

387   wet conditions (Mernild et al. 2014). Furthermore, runoff was negatively correlated to surface

388   albedo and snow cold content, as confirmed by Hanna et al. (2008) and Ettema et al. (2009).

17

389   For the dry North and Northeast Greenland (Table 1), the relatively low end-of-winter

390   snowpack melted relatively fast during spring warm-up. After the winter snowpack had ablated,

391   the ice surface albedo promoted a stronger radiation-driven ablation and surface runoff, owing to

392   the lower ice albedo. For the wetter Southeast Greenland (Table 1), the relatively high end-of-

393   winter snow accumulation, combined with frequent summer snow precipitation events, kept the

394   albedo high. Therefore, in that region it generally took longer time to melt the snowpack

395   compared to the drier parts of the GrIS before ablation started to affect the underlying glacier ice.

396   Regarding specific runoff (runoff volume per unit drainage area per time, $L\ s^{-1}\ km^{-2}$; to

397   convert to mm yr^{-1}, multiply by 31.6), maximum values of 16.7 $L\ s^{-1}\ km^{-2}$ and 22.9 $L\ s^{-1}\ km^{-2}$

398   were seen in Southwest Greenland for the mean 35-year and 2005–2014 periods, respectively.

399   The minimum values of 4.4 $L\ s^{-1}\ km^{-2}$ and 6.2 $L\ s^{-1}\ km^{-2}$ for the mean 35-year and 2005–2014

400   periods, respectively, occurred in Northeast Greenland (Table 2). On average for the GrIS, the

401   corresponding specific runoffs were 8.1 $L\ s^{-1}\ km^{-2}$ and 11.1 $L\ s^{-1}\ km^{-2}$, respectively, which are

402   within the range of previous studies (e.g., Mernild et al. 2008). Specific runoff is a valuable tool

403   for comparing runoff on regional and catchment scales, and it can also be used to quantifying the

404   absolute runoff contributions from increasing runoff and increasing melt area extent. The

405   difference in specific runoff between the two periods indicates that the increase in runoff has

406   increased faster than the increase in melt area extent.

407   Refreezing and retention in the snow and firn packs were defined as rain plus surface

408   melt minus runoff (see Section 2.4). For the GrIS, the 35-year mean refreezing and retention was

409   estimated to be 25 % (140.1 ± 35.5 Gt yr^{-1}), and it was 22 % (158.4 ± 34.4 Gt yr^{-1}) for 2005–

410   2014 (Table 1). Hence, refreezing and retention provided an important quantitative contribution

411   to the evolution of snow and firn layers, ice densities, snow temperatures (cold content or snow

412   temperatures below freezing), and moisture available for runoff (Liston and Mernild 2012). The

413   SnowModel ERA-I refreezing and retention simulations were within the order of magnitude

414   produced by the single-layer snowpack model used by Hanna et al. (2008), but lower than the 45

415   % simulated by Ettema et al. (2009). On the regional-scale, the 35-year mean refreezing and

416   retention value varied from 13 % in North Greenland to 30 % in both Southeast and Southwest

417   Greenland. For 2005–2014, the values were 12 % for North Greenland and 32 % for Southeast

418   Greenland (Table 1), indicating a clear variability in refreezing and retention between the

419   different regions.

420   In Figure 3a, the time series of GrIS mean annual refreezing and retention shows an

421   increasing trend (significant) and variability ranging from ~0.05 m w.e. (1992) to ~0.14 m w.e.

422   (2012), with an annual mean value of 0.09 ± 0.02 m w.e. In Figure 3b, the spatial 35-year mean

423   GrIS refreezing and retention is presented together with values from 1992 and 2012, the

424   minimum and maximum years, respectively. The mean spatial distribution highlights minimal

425   refreezing and retention at the GrIS interior, whereas areas with low elevation had values above

426   0.8 m w.e. in southern part of the GrIS. For the minimum year 1992, the pattern was more

427   pronounced with no refreezing and retention in the interior. The maximum year 2012 on the

428   other hand had refreezing and retention at the interior (between 0 and 0.02 m w.e.) (Figure 3b).

429   This was likely due to the extreme GrIS surface melt event throughout July 2012 (e.g., Nghiem

430   et al. 2012; Hanna et al. 2014). When divided into regions and catchments, the 2012 simulated

431   refreezing and retention showed a clear separation between highest values in Southwest

432   Greenland and lowest values in Northeast and East Greenland. Because here, refreezing and

433   retention were estimated as the sum of rain and melt minus the sum of runoff, this SnowModel

434   analysis did not provide a detailed description of the physical mechanisms and conditions

The Cryosphere
Discussions

Open Access

EGU

435   (beyond the standard SnowModel snowpack temperature and density evolution) leading to, e.g.,

436   non-linearities in snow and firn meltwater retention (Brown et al. 2012). However, while likely

437   an oversimplification of the natural system, this quantitative estimation of refreezing and

438   retention is an important step forward, and improves our runoff and the associated SMB

439   estimates. A model that does not include refreezing and retention processes in its snow and firn

440   evolution calculations, and the associated impacts on SMB, will introduce additional uncertainty

441   in it calculations of GrIS SMB and its contribution to sea-level change.

442   The GrIS SMB for the 35-year mean was 123.7 ± 163.2 Gt yr^{-1}, indicating a negative sea-

443   level contribution, and -42.9 ± 133.5 Gt yr^{-1} for 2005–2014, indicating a trend towards a positive

444   sea-level contribution (Table 1). This change in SMB between the two periods was mainly due to

445   an increase in runoff of 155.6 Gt yr^{-1}, where other water balance components showed relatively

446   lesser increases. For the GrIS, the 35-year mean SMB was negative for the northern regions,

447   positive for the southern regions and only positive for the southeastern sector for 2005–2014.

448   Overall, the SMB patterns were highly controlled by the distribution of precipitation and runoff.

449   The linear trends for the different water balance components are shown in Table 1. For

450   the 35-year period, only significant trends occurred for rain, surface melt, runoff, ablation, and

451   SMB (highlighted in bold in Table 1), where all except SMB showed positive trends (note that

452   SMB loss is calculated as negative by convention). In Figure 4, selected GrIS parameters are

453   illustrated, where, for example, SMB showed a negative trend of -99.2 Gt decade^{-1} (significant),

454   heading towards a zero balance at the end of the simulation period (Figure 4). For 2005–2014,

455   however, the SMB trend was positive 24.2 Gt decade^{-1} (insignificant). Similar positive SMB

456   trends have previously been shown in studies by Hanna et al. (2011), Tedesco et al. (2014),

457   Fettweis et al., (2008, 2011, 2013) and Wilton et al. (2016), even though variabilities in mean

458   SMB occur between the different studies. Wilton et al. (2016) estimated the GrIS SMB to be

459   ~100 Gt yr^{-1} in the late-2000s. Further, for 2005–2014, air temperature, precipitation, surface

460   melt, sublimation and evaporation, and runoff trends were all negative (insignificant) (Figure 4

461   and Table 1).

462

463   *4.2 Greenland spatiotemporal runoff distribution and EOF analysis*

464   The Greenland 35-year simulated catchment outlet runoff and specific runoff distribution

465   are shown in Figure 5. Each circle represents the volume (individual catchment outlet

466   hydrographs are not shown), including runoff from thousands of glaciers located between the

467   GrIS margin and the surrounding seas. The 35-year mean catchment outlet runoff varied from

468   <0.0001 to 25.7 × 10^9 m^3 (Figure 5a) and specific runoff from <0.1 to 127.5 L s^{-1} km^{-2} (Figure

469   5b). Catchment runoff variability depends on the regional climate conditions, land-ice area

470   cover, elevation range (including hypsometry) within each catchment, and catchment area. Here

471   the length in runoff season varied from two to three weeks in the north to four to six months in

472   the south. The median annual catchment runoff and specific runoff were 0.025 × 10^9 m^3 and 9.1

473   L s^{-1} km^{-2}, respectively. The median specific runoff value is in agreement with previous studies

474   (e.g., Mernild et al. 2010a). Further, the variance in catchment runoff and specific runoff varied

475   from <0.0001 to 8.3 × 10^9 m^3 and <0.01 to 19.3 L s^{-1} km^{-2}, respectively, with a median variance

476   of 0.006 × 10^9 m^3 and 2.4 L s^{-1} km^{-2} (Figures 4a and 4b). Regarding the linear trend in annual

477   runoff, both increasing and decreasing trends occurred over the 35 years. In total, 81 % (19 %) of

478   all catchments had increasing (decreasing) runoff trends over the 35 years (all of the decreasing

479   trends were insignificant). For western Greenland catchments, only increasing runoff trends

480   occurred (Figures 4a and 4b). The runoff and specific runoff trends varied among catchments

21

The Cryosphere
Discussions

Open Access

481   from -0.09 to 5.4×10^9 m^3 decade^{-1} and from -1.3 to 12.9 L s^{-1} km^{-2} decade^{-1}, respectively, with a

482   median value of 0.001×10^9 m^3 and 0.5 L s^{-1} km^{-2} decade^{-1} (Figures 4a and 4b).

483   The EOF analysis of runoff returned three axes that captured 25, 17 and 12 % of the

484   variation in runoff from the simulated SnowModel ERA-I annual catchment runoff (Figure 6).

485   Following several significance tests, only EOF1 captured significant variation. In Figure 6, the

486   temporal pattern in EOF1, with a 5-year running mean, reveals a pattern of positive running

487   mean values for the first two decades of the simulation period (1979–1999), and negative values

488   hereafter (2000–2014). When EOF1 is positive, Greenland runoff is relatively low and vice versa

489   (Figure 7). Overall, this indicates a positive temporal trend in runoff; as EOF1 goes down, runoff

490   goes up. While not significant based on EOF test metrics, EOF2 and EOF3 patterns are less

491   pronounced and in anti-phase to each other (Figure 6).

492   The temporal cycle of EOF patterns has associated spatial elements, derived from the

493   eigenvectors (Figure 8). The eigenvectors in Figure 8 reveal the spatial pattern as a correlation

494   between temporal trends captured by the EOFs and each individual Greenland catchment. These

495   data indicate that the temporal trend of increasing runoff captured in EOF1 is shared by nearly all

496   catchments in Greenland. Because decreasing EOF1 values indicate increasing runoff, a negative

497   correlation with EOF1 in space indicates increasing runoff. Catchment numbers greater than

498   #2500 (Figure 8) are located in Southeast Greenland and are in contrast to this. These catchments

499   experience a distinct out-of-phase pattern of runoff compared to the overall Greenland conditions

500   for the last 35 years.

501   This difference between Southeast Greenland and the rest of Greenland supports previous

502   findings (e.g., Lenaerts et al. 2015) proposing that variabilities in runoff are not only influenced

503   by melt conditions, but also by precipitation patterns (primarily the end-of-winter snow

22

504   accumulation), where high precipitation equals low runoff conditions such as in Southeast

505   Greenland. Furthermore, patterns were also detected to be associated to EOF2 and EOF3

506   (Figures 8b and 8c). These EOF2 and EOF3 patterns differed from EOF1, and they were

507   associated with a different geographic breakdown, where both positive and negative correlations

508   were seen for all regions. The physical mechanism behind these distributions is not clear.

509   There were strong correlations between the EOF1 and regional climate patterns expressed

510   by the AMO and NAO (Figure 9). We found a negative correlation between EOF1 and AMO (r

511    $= 0.68$; significant, $p<0.01$), suggesting that stronger AMO is associated with lower EOF1 values

512   which are indicative of higher runoff (Figure 9a). In contrast, we found a positive correlation

513   between EOF1 and NAO ($r = 0.40$; significant, $p<0.01$), suggesting that stronger NAO values

514   are associated with higher EOF1 values which are indicative of lower runoff (Figure 9b).

515   Additional insight into the time frame over which these correlations arises is seen in Figure 9.

516   For AMO, the lags are centered near zero, suggesting an immediate, real time correlation

517   between AMO and runoff. In contrast, the strongest lag in the NAO-EOF1 relationships is at -2,

518   suggesting a short delay in effects. Lags of 0 and -2 are not large, indicating that overall, large-

519   scale natural variability in AMO and NAO are closely associated in time to catchment runoff

520   variations in Greenland.

521   Mernild et al. (2011) emphasized that trends in AMO (smoothed) was analogous to trends

522   in GrIS melt extent, where increasing AMO equaled increasing melt extent, and vice versa.

523   Further, Chylek et al. (2010) showed that the Arctic detrended temperatures were highly

524   correlated with AMO. However, this issue requires further investigation to establish the details

525   of, and the mechanisms behind, the interrelationships.

526

5. Conclusions

527

528   Greenland catchment outlet runoff is rarely observed and studied, although quantification

529   of runoff from Greenland is crucial for our understanding of the link between a changing climate

530   and changes in the cryosphere, hydrosphere, and atmosphere. We have reconstructed the impact

531   of changes in climate conditions on hydrological processes at the surface of the GrIS for the 35-

532   year period 1979–2014. We have also simulated the Greenland spatiotemporal distribution of

533   refreezing and retention, and freshwater runoff to surrounding seas by merging SnowModel (a

534   spatially distributed meteorological, full surface energy balance, snow and ice evolution model)

535   with HydroFlow (a linear-reservoir run-off routing model) forced by ERA-I atmospheric forcing

536   data. Before simulating the individual catchment runoff to downstream areas, the catchment

537   divides and flow networks were estimated, yielding a total of 3,272 catchments in Greenland.

538   For the GrIS, the simulated spatial distribution and time series of surface hydrological

539   processes were in accordance with previous studies, although precipitation and SMB were in the

540   lower range of these studies. Overall, Greenland has warmed and the runoff from Greenland has

541   increased in magnitude. Specifically, 81 % of the catchments showed increasing runoff trends

542   over the simulation period, with relatively high and low mean catchment runoff from the

543   southwestern and northern parts of Greenland, respectively. This indicates distinct regional-scale

544   runoff variability in Greenland. Runoff variability with near zero lag time suggests a real-time

545   covariation between the pattern in EOF1 and changes in AMO and NAO. This indicates that

546   large-scale natural variability in AMO and NAO is closely related to catchment runoff variations

547   in Greenland. The physical mechanism behind this phenomenon is unclear, unless it is a response

548   to "long-term" cycles in AMO and NAO.

549   The simulated runoff can be used as boundary conditions in ocean models to understand

550   hydrologic links between terrestrial and marine environments in the Arctic. Changes and

551   variability in runoff from Greenland are expected to play an essential role in the hydrographic

552   and circulation conditions in fjords and the surrounding ocean under a changing climate.

553

554   **Acknowledgements**

559

560

561

562

563

564

565

566

567

568

569

570

571

572

573

574

575

The Cryosphere
Discussions

576 **References**

577 AMAP, 2017. Snow, Water, Ice and Permafrost. Summary for Policy-makers. Arctic Monitoring

578 and Assessment Programme (AMAP), Oslo, Norway, 20 pp.

579

580 Bales, R. C., Guo, Q., Shen, D., McConnell, J. R., Du, G., Burkhart, J. F., Spikes, V. B., Hanna,

581 E., and Cappelen, J. 2009. Annual accumulation for Greenland updated using ice core data

582 developed during 2000–2006 and analysis, of daily coastal meteorological data. J. Geophys.

583 Res., 114, D06116, doi:10.1029/2008JD011208.

584

585 Bamber, J., van den Broeke, M., Ettema, J., Lenaerts, J., and Rignot, E., 2012. Recent large

586 increases in freshwater fluxes from Greenland into the North Atlantic. *Geophys. Res. Letts.*, 39,

587 L19501, doi:10.1029/2012GL052552.

588

589 Banwell, A., Hewitt, I., Willis, I., and Arnold, N. 2016. Moulin density controls drainage

590 development beneath the Greenland ice sheet. J. Geophys. Res. Earth Surf., 121, 2248–2269.

591

592 Bartholomew, I., Nienow, P., Mair, D., Hubbard, A., King, M. A., and Sole, A. 2010. Seasonal

593 evolution of subglacial drainage and acceleration in a Greenland outlet glacier. Nat. Geosci.,

594 3(6), 408–411.

595

596 Bartholomew, I., Nienow, P., Sole, A., Mair, D., Cowton, T., and King, M. 2012. Short-term

597 variability in Greenland ice sheet motion forces by time-varying meltwater drainage:

598 Implications for the relationship between subglacial drainage system behavior and ice velocity. J.

599 Geophys. Res., 117, F03002, doi:10.1029/2011JF002220.

600

601 Beamer, J. P., Hill, D. F., Arendt, A., and Liston, G. E. 2016. High-resolution modeling of

602 coastal freshwater discharge and glacier mass balance in the Gulf of Alaska watershed. Water

603 Resour. Res., 52, 3888–3909, doi:10.1002/2015WR018457.

604

605 Bliss, A., Hock, R., and Radić, V. 2014. Global response of glacier runoff to twenty-first century

606 climate change, J. Geophys. Res. Earth Surf., 119, doi:10.1002/2013JF002931.

607

608   Box, J. E. 2013. Greenland ice sheet mass balance reconstruction, Part II: Surface mass balance

609   (1840–2010). Journal of Climate, 26, 6974–6989, doi:10.1175/JCLI-D-12-00518.1.

610

611   Box, J. E., Cappelen, J., Chen, C., Decker, D., Fettweis, X., Mote, T., Tedesco, M., van de Wal,

612   R. S. W., and Wahr, J. 2012. Greenland Ice Sheet. In Jeffries, M. O., Richter-Menge, J. A., and

613   Overland, J. E. (Eds). Arctic Report Card 2012, http://www.arctic.noaa.gov/reportcard.

614

615   Brown, J., Bradford, J., Harper, J., Pfeffer, W. T., Humphrey, N., and Mosley-Thompson, E.,

616   2012. Georadar-derived estimates of firn density in the percolation zone, western Greenland ice

617   sheet. *Journal of Geophysical Research*, 117, F01011, doi:10.1029/2011JF002089.

618

619   Carrivick, J. L., and Quincey, D. J., 2014. Progressive increase in number and volume of ice-

620   marginal lakes on the western margin of the Greenland Ice Sheet. *Global and Planetary Change*,

621   116, 156-163, doi:10.1016/j.gloplacha.2014.02.009.

622

623   Chen, X., Zhang, X., Church, J. A., Watson, C. S., King, M. A., Monselesan, D., Legresy, B.,

624   and Harig, C. 2017. The increasing rate of global mean sea-level rise during 1993–2014. Nature

625   Climate Change, doi:10.1038/nclimate3325.

626

627   Chu, W., Creyts, T., and Bell, R. E., 2016. Rerouting of subglacial water flow between

628   neighboring glaciers in West Greenland. J. Geophys. Res. Earth Surf., 121, 925–938.

629

630   Church, J. A., Clark, P. U., Cazenave, A., Gregory, J. M., Jevrejeva, S., Levermann, A.,

631   Merrifield, M. A., Milne, G. A., Nerem, R. S., Nunn, P. D., Payne, A. J., Pfeffer, W. T.,

632   Stammer, D., and Unnikrishnan, A. S. 2013. Sea Level Change. In: Climate Change 2013: The

633   Physical Science Basis. Contribution of Working Group I to the Fifth Assessment Report of the

634   Intergovernmental Panel on Climate Change [Stocker, T.F., Qin, D., Plattner, G.-K., Tignor, M.,

635   Allen, S.K., Boschung, J., Nauels, A., Xia, Y., Bex, V. and, Midgley, P.M. (eds.)]. Cambridge

636   University Press, Cambridge, United Kingdom and New York, NY, USA.

637

The Cryosphere
Discussions

638   Chylek, P., C.K. Folland, G. Lesins and M.K. Dubey. 2010. Twentieth century bipolar seesaw of

639   the Arctic and Antarctic surface air temperatures. Geophys. Res. Lett., 37(8), L08703,

640   doi:10.1029/2010GL042793.

641

642   Cuffey, K. M. and Paterson, W. S. B. 2010. The Physics of Glaciers. Fourth Edition. Elsevier,

643   pp. 693.

644

645   Cullather R. I., Nowicki, S. M. J., Zhao, B., and Koenig, L. S. 2016. A Characterization of

646   Greenland Ice Sheet Surface Melt and Runoff in Contemporary Reanalyses and a Regional

647   Climate Model. Front. Earth Sci., 4(10), doi:10.3389/feart.2016.00010.

648

649   Dee, D. P., Uppala, S. M., Simmons, A. J., Berrisford, P., Poli, P., Kobayashi, S., Andrae, U.,

650   Balmaseda, M. A., Balsamo, G., Bauer, P., Bechtold, P., Beljaars, A. C. M., van de Berg, L.,

651   Bidlot, J., Bormann, N., Delsol, C., Dragani, R., Fuentes, M., Geer, A. J., Haimberger, L., Healy,

652   S. B., Hersbach, H., Holm, E. V., Isaksen, L., Kållberg, P., Kohler, M., Matricardi, M., McNally,

653   A. P., Monge-Sanz, B. M., Morcrette, J.-J., Park, B.-K., Peubey, C., de Rosnay, P., Tavolato, C.,

654   Thepaut, J.-N., Vitart, F. 2011. The ERA-Interim reanalysis: configuration and performance of

655   the data assimilation system. Q. J. R. Meteorol. Soc., 137, 553–597, doi:10.1002/qj.828.

656

657   Dickson, R. R., Osborn, T. J., Hurrell, J. W., Meincke, J., Blindheim, J., Adlandsvik, B., Vinje,

658   T., Alekseev, G., and Maslowski, W. 2000. The Arctic Ocean response to the North Atlantic

659   Oscillation. Journal of Climate, 13, 2671–2696.

660

661   Enderlin, E. M., Howat, I. M., Jeong, S., Hoh, M.-J., van Angelen, J. H., and van den Broeke, M.

662   R. 2014. An improved mass budget for the Greenland ice sheet. Geophysical Research Letters,

663   41(3), 866–872.

664

665   Ettema, J., van den Broeke, M. R., van Meijgaard, E., van den Berg, W. J., Bamber, J. L., Box, J.

666   E., and Bales, R. C. 2009. Higher surface mass balance of the Greenland ice sheet revealed by

667   high-resolution climate modeling. Geophysical Research Letters, 36, L12501.

668

The Cryosphere

Discussions

Open Access

EGU

669   Everett, A., Murray, T., Selmes, N., Rutt, I. C., Luckman, A., James, T. D., Clason, S., O´Leary,

670   M., Karunarathna, H., Moloney, V., and Reeve, D. E. 2016. Annual down-glacier drainage of

671   lakes and water-filled crevasses at Helheim Glacier, southeast Greenland. J. Geophys. Res. Earth

672   Surf., 121, 1819–1833.

673

674   Fettweis, X., Box, J. E., Agosta, C., Amory, C., Kittel, C., Lang, C., van As, D., Machguth, H.,

675   and Gallée, H., 2017. Reconstructions of the 1900–2015 Greenland ice sheet surface mass

676   balance using the regional climate MAR model. The Cryosphere, 11, 1015–1033, doi:10.5194/tc-

677   11-1015-2017.

678

679   Fettweis, X., Franco, B., Tedesco, M., van Angelen, J. H., Lenaerts, J. T. M., van den Broeke, M.

680   R., and Gallée, H., 2013. Estimating the Greenland ice sheet surface mass balance contribution to

681   future sea level rise using the regional atmospheric climate model MAR. The Cryosphere, 7, 709

682   469–489.

683

684   Fettweis, X., Hanna, E., Gallée, H., Huybrechts, P., and Erpicum, M. 2008. Estimation of the

685   Greenland ice sheet surface mass balance for the 20th and 21st centuries, The Cryosphere, 2,

686   117–129, doi:10.5194/tc-2-117-2008.

687

688   Fettweis, X., Tedesco, M., van den Broeke, M., and Ettema, J., 2011. Melting trends over the

689   Greenland ice sheet (1958–2009) from spaceborne microwave data and regional climate models.

690   The Cryosphere, 5, 359–375.

691

692   Goodison, B. E., Sevruk, B., and Klemm, S. 1989.WMO solid precipitation measurement

693   intercomparison: objectives, methodology, analysis. IAHS publication, 179, 57–64.

694

695   Hanna, E., Fettweis, X., Mernild, S. H., Cappelen, J., Ribergaard, M., Shuman, C., Steffen, K.,

696   Wood, L., and Mote, T. 2014. Atmospheric and oceanic climate forcing of the exceptional

697   Greenland Ice Sheet surface melt in summer 2012. *International Journal of Climatology*, 34,

698   1022–1037.

699

The Cryosphere
Discussions

Open Access

EGU

700   Hanna, E., Huybrechts, P., Cappelen, J., Steffen, K., Bales, R., Burgess, E., McConnell, J.,

701   Steffensen, J. P., Van den Broeke, M., Wake, L., Bigg, B., Griffiths, M., and Savas, D. 2011.

702   Greenland Ice Sheet surface mass balance 1870 to 2010 based on Twentieth Century Reanalysis,

703   and links with global climate forcing, Journal of Geophysical Research, 116, D24121,

704   doi:10.1029/2011JD016387.

705

706   Hanna, E., Huybrechts, P., Steffen, K., Cappelen, J., Huff, R., Shuman, C., Irvine-Fynn, T.,

707   Wise, S., and Griffiths, M. 2008. Increased runoff from melt from the Greenland ice sheet: A

708   response to global warming. Journal of Climate, 21, 331–341.

709

710   Hanna, E., McConnell, J., Das, S., Cappelen, J., and Stephens, A. 2006. Observed and modelled

711   Greenland Ice Sheet snow accumulation, 1958–2003, and links with regional climate forcing.

712   Journal of Climate, 19(3), 344–358, doi:10.1175/JCLI3615.1.

713

714   Hanna, E., Navarro, F. J., Pattyn, F., Domingues, C., Fettweis, X., Ivins, E., Nicholls, R. J., Ritz,

715   C., Smith, B., Tulaczyk, S., Whitehouse, P., and Zwally, J. 2013. Ice-sheet mass balance and

716   climate change. Nature, 498, 51–59.

717

718   Hanna, E., Mernild, S. H., Cappelen, J., and Steffen, K. 2012. Recent warming in Greenland in a

719   long-term instrumental (1881–2012) climatic context. Part 1: Evaluation of surface air

720   temperature records. Environmental Research Letters, 7, 045404, doi:10.1088/1748-

721   9326/7/4/045404.

722

723   Haper, J., Humphrey, N., Pfeffer, W. T., Brown, J. and Fettweis, X. 2012. Greenland ice-sheet

724   contribution to sae-level rise buffered by meltwater storage in firn. Nature, 22117–22124.

725

726   Hasholt, B., Mikkelsen, A. B., Nielsen, H. M, and Larsen, M. A. D. 2013. Observations of

727   Runoff and Sediment and Dissolved Loads from the Greenland Ice Sheet at Kangerlussuaq, West

728   Greenland, 2007 to 2010. Zeitschrift für Geomorphologie, 57(2), 3–27, doi:10.1127/0372-

729   8854/2012/S-00121.

730

731   Hewitt, I. 2013. Seasonal changes in ice sheet motion due to melt water lubrication. Earth Plant.

732   Sci. Lett., 371–372, 16–25.

733

734   Hiemstra, C. A., Liston, G. E., and Reiners, W. A. 2006. Observing, modelling, and validating

735   snow redistribution by wind in a Wyoming upper treeline landscape. Ecol. Model. 197, 35–51,

736   doi: 10.1016/j.ecolmodel.2006.03.005.

737

738   Howat, I. M., De la Peña, S., Van Angelen, J. H., Lenaerts, J. T. M., and Van den Broeke, M. R.

739   2013. Expansion of meltwater lakes on the Greenland Ice Sheet. The Cryosphere, 7, 201-204.

740   doi:10.5194/tc-7-201-2013.

741

742   Hurrell, J. W. 1995. Decadal trends in the North Atlantic Oscillation: regional temperatures and

743   precipitation. Science, 269, 676–679. doi:10.1126/science.269.5224.676.

744

745   Hurrell, J. W. and van Loon, H. 1997. Decadal variations in climate associated with the North

746   Atlantic oscillation, Climate Change, 36, 301–326.

747

748   Kaplan, A., Cane, M. A., Kushnir, Y. and Clement, A. C. 1998. Analyses of global sea surface

749   temperatures 1856–1991. Journal of Geophysical Research, 103, 18575–18589.

750

751   Kobayashi, S., Ota, Y., Harada, Y., Ebita, A., Moriya, M., Onoda, H., Onogi, K., Kamahori, H.,

752   Kobayashi, C., Endo, H., Miyaoka, K., and Takahashi, K. 2015. The JRA-55 Reanalysis:

753   General Specifications and Basic Characteristics, J. Meteorol. Soc. Jpn., 93, 5–48,

754   doi:10.2151/jmsj.2015-001.

755

756   Kohler, T. J., Zarsky, J. D., Yde, J. C., Lamarche-Gagnon, G., Hawkings, J. R., Tedstone, A. J.,

757   Wadham, J. L., Box, J. E., Beaton, A., and Stibal, M., 2017. Carbon dating reveals seasonal

758   shifts in the source of sediments exported from the Greenland Ice Sheet. Geophys. Res. Lett.,

759   44(12), 6209–6217.

760

The Cryosphere

Discussions

Open Access

EGU

761 Koziol, C., Arnold, N., Pope, A., and Colgan, W., 2017. Quantifying supraglacial meltwater

762 pathways in the Paakitsoq region, West Greenland. J. Glaciol., 63(239), 464–476.

763

764 Langen, P. L., Mottram, R. H., Christensen, J. H., Boberg, F., Rodehacke, C. B., Stendel, M., van

765 As, D., Ahlstrøm, A. P., Mortensen, J., Rysgaard, S., Petersen, D., Svendsen, K. H.,

766 Algeirsdottir, G. A., and Cappelen, J. 2015. Quantifying Energy and Mass Fluxes Controlling

767 Godthåbsfjord Freshwater Input in a 5-km Simulation (1991–2012). Journal of Climate, 28,

768 3694–3713, doi:10.1175/JCLI-D-14-00271.1.

769

770 Lenaerts, J. T. M., Le Bars, D., van Kampenhout, L., Vizcaino, M., Enderlin, E. M., and van den

771 Broeke, M. R. 2015. Representing Greenland ice sheet freshwater fluxes in climate models.

772 Geophys. Res. Lett., 42, 6373–6381, doi:10.1002/2015GL064738.

773

774 Levinsen, J. F., Forsberg, R., Sørensen, L. S., and Khan, S. A. 2015. Essential Climate Variables

775 for the Ice Sheets from Space and Airborne measurements. Danmarks Tekniske Universitet

776 (DTU) PhD Thesis, Kgs. Lyngby, pp. 1–232.

777

778 Lewis, S. M., and Smith, L. C. 2009. Hydrological drainage of the Greenland ice sheet. Hydrol.

779 Processes, 23, 2004–2011, doi:10.1002/hyp.7343.

780

781 Liston, G. E. 1995. Local advection of momentum, heat, and moisture during the melt of patchy

782 snow covers. J. Appl.Meteorol., 34, 1705–1715, doi:10.1175/1520-0450-34.7.1705.

783

784 Liston, G. E. and Elder, K. 2006a. A distributed snow-evolution modeling system (SnowModel).

785 J. Hydrometeorol., 7, 1259–1276, doi:10.1175/JHM548.1.

786

787 Liston, G. E. and Elder, K. 2006b. A meteorological distribution system for high-resolution

788 terrestrial modeling (MicroMet). J. Hydrometeorol., 7, 217–234, doi:10.1175/JHM486.1.

789

790 Liston, G. E., Haehnel, R. B., Sturm, M., Hiemstra, C. A., Berezovskaya, S., and Tabler, R. D.

791 2007. Simulating complex snow distributions in windy environments using SnowTran-3D. J.

792 Glaciol., 53, 241–256.

793

794 Liston, G. E. and Hiemstra, C. A. 2011. The changing cryosphere: pan-Arctic snow trends

795 (1979–2009). J. Clim., 24, 5691–5712.

796

797 Liston, G. E. and Mernild, S. H. 2012. Greenland freshwater runoff. Part I: a runoff routing

798 model for glaciated and non-glaciated landscapes (HydroFlow). J. Clim., 25(17), 5997–6014.

799

800 Liston, G. E. and Sturm, M. 1998. A snow-transport model for complex terrain. J. Glaciol., 44,

801 498–516.

802

803 Liston, G. E. and Sturm, M. 2002.Winter precipitation patterns in Arctic Alaska determined from

804 a blowing-snow model and snow depth observations. J. Hydrometeorol., 3, 646–659.

805

806 Liston, G. E., Winther, J.-G., Bruland, O., Elvehøy, H., and Sand, K. 1999. Below surface ice

807 melt on the coastal Antarctic ice sheet. J. Glaciol., 45, 273–285.

808

809 Machguth, H., MacFerrin, M., van as, D., Box, J., Charalampidis, C., Colgan, W., Fausto, R. S.,

810 Meijer, H. A. J., Mosley-Yhompson, E., and van de Wal, R. S. W. 2016. Greenland meltwater

811 storage in firn limited by near-surface ice formation. Nature Climate Change, 6(4), 390–393,

812 doi.org/10.1038/nclimate2899.

813

814 Mernild, S. H., B. Hasholt and G. E. Liston 2006b. Water flow through Mittivakkat Glacier,

815 Ammassalik Island, SE Greenland. Geografisk Tidsskrift-Danish Journal of Geography, 106(1),

816 25–43.

817

818 Mernild, S. H., Hanna, E., McConnell, J. R., Sigl, M., Beckerman, A. P., Yde, J. C., Cappelen, J.,

819 and Steffen, K. 2015. Greenland precipitation trends in a long-term instrumental climate context

820   (1890–2012): Evaluation of coastal and ice core records. International Journal of Climatology,

821   35, 303–320, doi:10.1002/joc.3986.

822

823   Mernild, S. H. and Liston, G. E. 2010. The influence of air temperature inversion on snow melt

824   and glacier surface mass-balance simulations, SW Ammassalik Island, SE Greenland. Journal of

825   Applied Meteorology and Climate, 49(1), 47–67.

826

827   Mernild, S. H. and Liston, G. E. 2012. Greenland freshwater runoff. Part II: distribution and

828   trends, 1960–2010. J. Clim., 25(17), 6015–6035.

829

830   Mernild, S. H., Liston, G. E., Hasholt, B., and Knudsen, N. T. 2006a. Snow distribution and melt

831   modeling for Mittivakkat Glacier, Ammassalik Island, SE Greenland. Journal of

832   Hydrometeorology, 7, 808–824.

833

834   Mernild, S. H., and Liston, G. E., and Hiemstra, C. A. 2014. Northern hemisphere glaciers and

835   ice caps surface mass balance and contribution to sea-level rise. J. Clim., 27(15), 6051–6073,

836   doi:10.1175/JCLI-D-13-00669.1.

837

838   Mernild, S. H., Liston, G. E., Hiemstra, C. A. and Christensen, J. H. 2010a. Greenland Ice Sheet

839   surface mass-balance modeling in a 131 year perspective 1950–2080. Journal of

840   Hydrometeorology, 11(1), 3–25, doi.org/10.1175/2009JHM1140.1.

841

842   Mernild, S. H., Liston, G. E., Hiemstra, C. A., and Steffen, K. 2008. Surface Melt Area and

843   Water Balance Modeling on the Greenland Ice Sheet 1995–2005. Journal of Hydrometeorology,

844   9(6), 1191–1211, doi.org/10.1175/2008JHM957.1.

845

846   Mernild, S. H., Liston, G. E., van As, D., Hasholt, B., and Yde, J. C. 2017. High-resolution ice

847   sheet surface mass-balance and spatiotemporal runoff simulations: Kangerlussuaq, West

848   Greenland. Accepted Arctic, Antarctic, and Alpine Research (Special Issue, Kangerlussuaq).

849

The Cryosphere

Discussions

Open Access

EGU

850 Mernild, S. H., Mote, T., and Liston, G. E. 2011. Greenland Ice Sheet surface melt extent and
851 trends, 1960–2010. Journal of Glaciology, 57(204), 621–628.

852

853 Metcalfe, J. R., Ishida, S., and Goodison, B. E. 1994. A corrected precipitation archive for the
854 Northwest Territories of Canada,
855 http://www.usask.ca/geography/MAGS/Data/Public_Data/precip_corr/pcpncor_e.htm.

856

857 Nghiem, S. V., Hall, D. K., Mote, T. L., Tedesco, M., Albert, M. R., Keegann, K., Shuman, C.
858 A., DiGirolamo, N. E., and Neumann, G. 2012. The extreme melt across the Greenland ice sheet
859 in 2012. *Geophysical Research Letters*, 39, L20502.

860

861 Nick, F. M., Vieli, A., Howat, I. M., and Joughin, I. R. 2009. Large-scale changes in Greenland
862 outlet glacier dynamics triggered at the terminus. Nature Geoscience, 2(2), 110–114,
863 doi:10.1038/ngeo394.

864

865 Noël, B., van de Berg, W. L., Lhermitte, S., Wouters; B., Machguth, H., Howat, I., Citterio, M.,
866 Moholdt, G., Lenaerts, J. T. M., and van den Broeke, M. R. 2017. A tipping point in refreezing
867 accelerates mass loss of Greenland's glaciers and ice caps. Nature Communications, 8, 1–8,
868 doi:10.1038/ncomms14730.

869

870 Overland, J. E., Francis, J., Hanna, E. and Wang, M. 2012. The recent shift in early summer
871 arctic atmospheric circulation. Geophysical Research Letters, 39, L19804.

872

873 Preisendorfer, R.W. 1998. Principal Component Analysis in Meteorology and Oceanography. In:
874 Mobley, C.D. (Ed.) Elsevier, Amsterdam, p. 452.

875

876 Rahmstorf, S., and Coauthors. 2005. Thermohaline circulation hysteresis: A model
877 intercomparison. Geophys. Res. Lett., 32, L23605, doi:10.1029/2005GL023655.

878

879 Rasmussen, R., Baker, B., Kochendorfer, J., Meyers, T., Landolt, S., Fischer, A. P., Black, J.,
880 Theriault, J. M., Kucera, p., Gochis, D., Smith, C., Nitu, R., Hall, M., Ikeda, K., and Gutmann,

881   E. 2012. How well are we measuring snow? The NOAA/FAA/NCAR Winter Precipitation Test

882   Bed. BAMS, 811–829.

883

884   Rignot, E. and Mouginot, J. 2012. Ice flow in Greenland for the International Polar Year 2008–

885   2009. Geophysical Research Letters, 39, L11501, doi:10.1029/2012GL051634.

886

887   Rignot, E., Velicogna, I., van den Broeke, M. R., Monaghan, A., and Lenaerts, J. 2011.

888   Acceleration of the contribution of the Greenland and Antarctic ice sheets to sea level rise.

889   Geophysical Research Letters, 38, L05503.

890

891   Roberts, M.J. 2005. Jökulhlaups: a reassessment of floodwater flow through glaciers. *Rev.*

892   *Geophys.,* 43(1), RG1002, doi:10.1029/2003RG000147.

893

894   Rogers, A. N., Bromwich, D. H., Sinclair, E. N. and Cullather, R. I., 2001. The atmospheric

895   hydrological cycle over the Arctic basins from reanalysis. Part II: Inter-annual variability.

896   Journal of Climate, 14, 2414–2429.

897

898   Selmes, N., Murray, T., and James, T. D. 2011. Fast draining lakes on the Greenland ice sheet.

899   Geophys Res. Lett., 38(15), doi:10.1029/2011GL047872.

900

901   Shepherd, A. et al. 2012. A Reconciled Estimate of Ice-Sheet Mass Balance. Science, 338,

902   1183–1189.

903

904   Sparnocchia S, Pinardi N, and Demirov E. 2003. Multivariate empirical orthogonal function

905   analysis of the upper thermocline structure of the Mediterranean Sea from observations and

906   model simulations. Ann. Geophys, 21, 167–187.

907

908   Sugden, D.E., Clapperton, C. M, and Knight, P. G.1985. A jökulhlaup near Søndre Strømfjord,

909   West Greenland, and some effects on the ice-sheet margin. Journal of Glaciology, 31(109), 366–

910   368.

911

912   Steffen, K. 1995. Surface energy exchange at the equilibrium line on the Greenland ice sheet

913   during onset of melt. Annals of Glaciology, 21, 13–18.

914

915   Straneo, F., Curry,R. G., Sutherland, D. A., Hamilton, G. S., Cenedese, C., Våge, K., and Sterns,

916   L. A. 2011. Impact of fjord dynamics and glacial runoff on the circulation near Helheim Glacier.

917   Nat.Geosci., 4, 322–327, doi:10.1038/ngeo1109.

918

919   Tedesco, M., Willis, I. C., Hoffman, M. J., Banwell, A. F., Alexander, P., and Arnold, N. S.

920   2013. Ice dynamic response to two modes of surface lake drainage on the Greenland ice sheet.

921   Environ. Res. Lett., 8(3), 34007, doi:10.1088/1748-9326/8/3/034007.

922

923   Tedesco, M., Box, J. E., Cappelen, J., Fettweis, X., Mote. T., van de Wal, R. S. W., Smeets, C. J.

924   P. P., and Wahr, J. 2014. Greenland Ice Sheet. In Jeffries, M. O., Richter-Menge, J. A., and

925   Overland, J. E. (eds.). Arctic Report Card 2014.

926

927   Tedesco, M., Box, J. E., Cappelen, J., Fausto, R. S., Fettweis, X., Mote, T., Smeets C. J. P. P.,

928   van As, D., Velicogna, I., van de Wal, R. S. W. and Wahr, J. 2016. Greenland Ice Sheet. In

929   Richter-Menge, J. A., Overland, J. E., and Mathis, J. T. (eds.). Arctic Card Report 2016.

930

931   Uppala, S. M., Kållberg, P. W., Simmons, A. J., Andrae, U., Da Costa Bechtold, V., Fiorino, M.,

932   Gibson, J.K., Haseler, J., Hernandez, A., Kelly, G. A., Li, X., Onogi, K., Saarinen, S., Sokka,

933   N., Allan, R. P., Anderson, E., Arpe, K., Balmaseda, M. A., Beljaars, A. C. M., Van De Berg, L.,

934   Bidlot, J., Bormann, N., Caires, S., Chevallier, F., Dethof, A., Dragosavac, M., Fisher, M.,

935   Fuentes, M., Hagemann, S., Hólm, E., Hoskins, B. J., Isaksen, L., Janssen, P. A. E. M., Jenne, R.,

936   Mcnally, A. P., Mahfouf, J.-F., Morcrette, J.-J., Rayner, N. A., Saunders, R.W., Simon, P., Sterl,

937   A., Trenbreth, K. E., Untch, A., Vasiljevic, D., Viterbo, P., and Woollen, J.: The ERA-40 re-

938   analysis, Q. J. Roy. Meteor. Soc., 131, 2961–3012, doi:10.1256/qj.04.176, 2005.

939

940   van Angelen, J. H., Lenaerts, J. T. M., van den Broeke, J. T. M., Fettweis, X., van Meijgaard, E.

941   2013. Rapid loss of firn pore space accelerates 21 century Greenland mass loss. Geophysical

942   Research Letter, 40, 2109–2113.

943

944   van As., D, Box, J. E., and Fausto, R. S., 2016: Challenges of Quantifying Meltwater Retention

945   in Snow and Firn: An Expert Elicitation. Frontiers in Earth Science, 4(101), 1–5.

946

947   van den Broeke, M., Smeets, P., Ettema, J., and Munneke, P. K. 2008a. Surface radiation balance

948   in the ablation zone of the west Greenland ice sheet, J. Geophys. Res., 113, D13105,

949   doi:10.1029/2007/JD009283.

950

951   van den Broeke, M., Smeets, P., Ettema, J., van der Veen, C., van de Wal, R., and Oerlemans, J.

952   2008b. Partitioning of melt energy and meltwater fluxes in the ablation zone of the west

953   Greenland ice sheet, The Cryosphere, 2, 179–189, doi:10.5194/tc-2-179-2008.

954

955   van de Wal, R. S. W., Greuell, W., van den Broeke, M. R., Reijmer, C. H., and Oerlemans, J.

956   2005. Surface mass-balance observations and automatic weather station data along a transect

957   near Kangerlussuaq, West Greenland, Ann. Glaciol., 42, 311–316.

958

959   van de Wal, R. S. W., Boot, W., van den Broeke, M., Smeets, C. J. P. P., Reijmer, C. H., Donker,

960   J. J. A., and Oerlemans, J. 2008. Large and rapid melt-induced velocity changes in the ablation

961   zone of the Greenland ice sheet. Science, 321, 111–113.

962

963   van der Veen, C. J. 2007. Fracture propagation as a means of rapidly transferring surface

964   meltwater to the base of glaciers. Geophys. Res. Lett., 34, L01501.

965

966   Weijer, W.,M. E. Maltrud, M. W. Hecht, H. A. Dijkstra, and M. A. Kliphuis, 2012. Response of

967   the Atlantic Ocean circulation to Greenland Ice Sheet melting in a strongly-eddying ocean

968   model. Geophys. Res. Lett., 39, L09606, doi:10.1029/2012GL051611.

969

970   Wilton, D. J., Jowett, A., Hanna, E., Bigg, G. R., van den Broeke, M. R., Fettweis, X., and

971   Huybrechts, P., 2017. High resolution (1 km) positive degree-day modelling of Greenland ice

972   sheet surface mass balance, 1870-2012 using reanalysis data. Journal of Glaciology, 63(237),

973   176–193.

974

975   Yang, D., Ishida, S., Goodison, B. E., and Gunter, T. 1999. Bias correction of daily precipitation

976   measurements for Greenland. J. Geophys. Res. 104(D6), 6171–6181,

977   doi:10.1029/1998JD200110.

978

979   Zwally, H. J., Abdalati, W., Herring, T., Larson, K., Saba, J., and Steffen, K. 2002. Surface melt-

980   induced acceleration of Greenland ice-sheet flow. Science, 297, 218–222.

981

982

983

984

985

986

987

988

989

990

991

992

993

994

995

996

997

998

999

1000
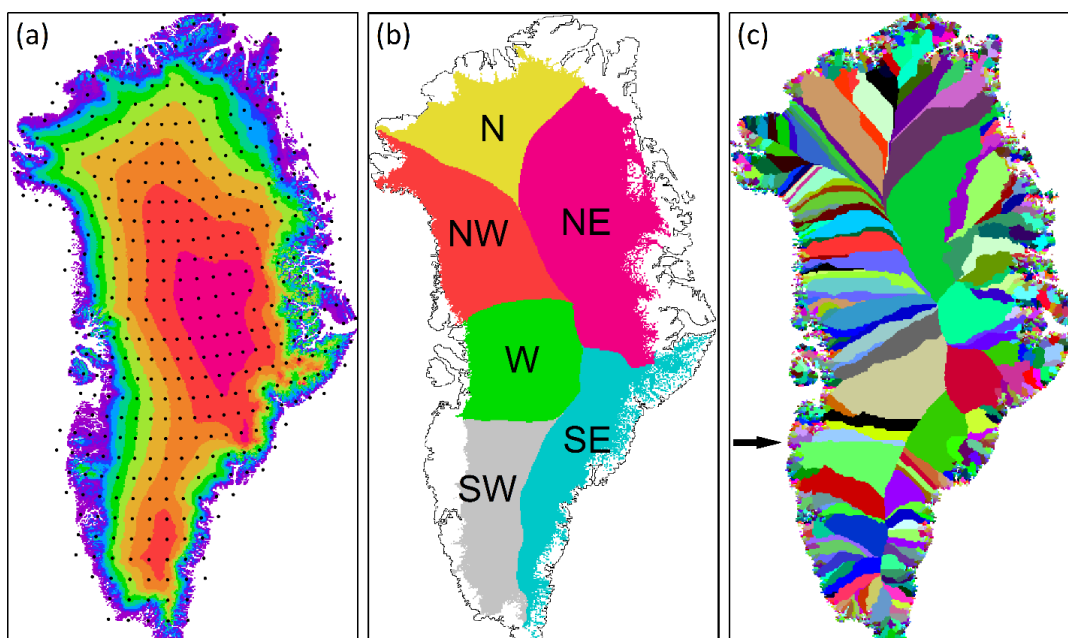
1001

Figure 1: (a) Greenland simulation domain with topography (500-m contour interval) and
locations of ERA-I atmospheric forcing grid points used in the model simulations (black dots; to
improve clarity only every other grid point was plotted in x and y, i.e., 25 % of the grid points
used are shown); (b) the major regional division of the GrIS following Rignot et al.
(unpublished); and (c) HydroFlow simulated individual Greenland drainage catchments ($n =$
3,272; represented by multiple colors). The approximate location of the Kangerlussuaq
catchment is shown with a black arrow.

1009

1010

1011

1012

1013
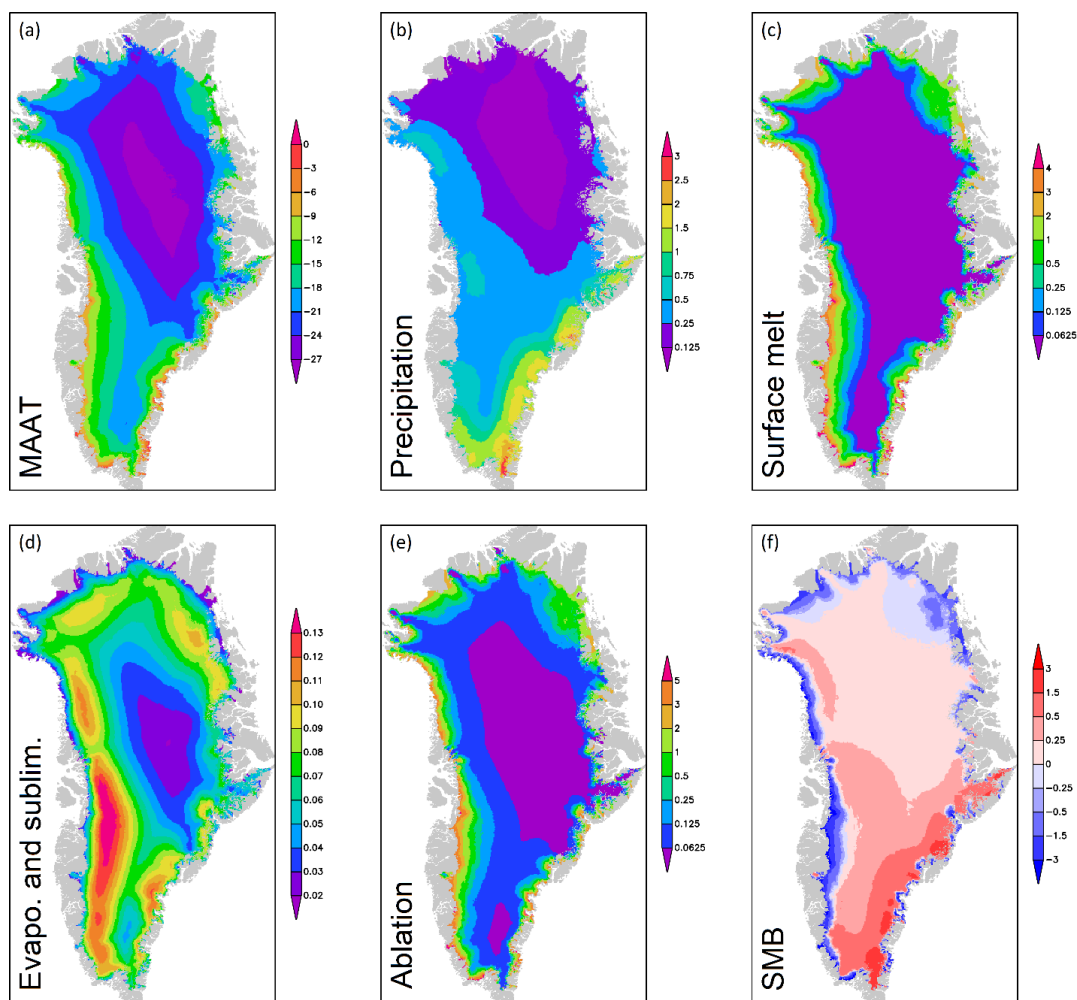
1014

Figure 2: SnowModel ERA-I simulated 35-year mean spatial GrIS surface (1979–2014): (a)
MAAT (°C); (b) precipitation (m w.e.); (c) surface melt (snow and ice melt) (m w.e.); (d)
evaporation and sublimation (m w.e.); (e) ablation (m w.e.); and (f) SMB (m w.e.).

1015

1016

1017

1018

1019

1020

1021

1022

1023

1024
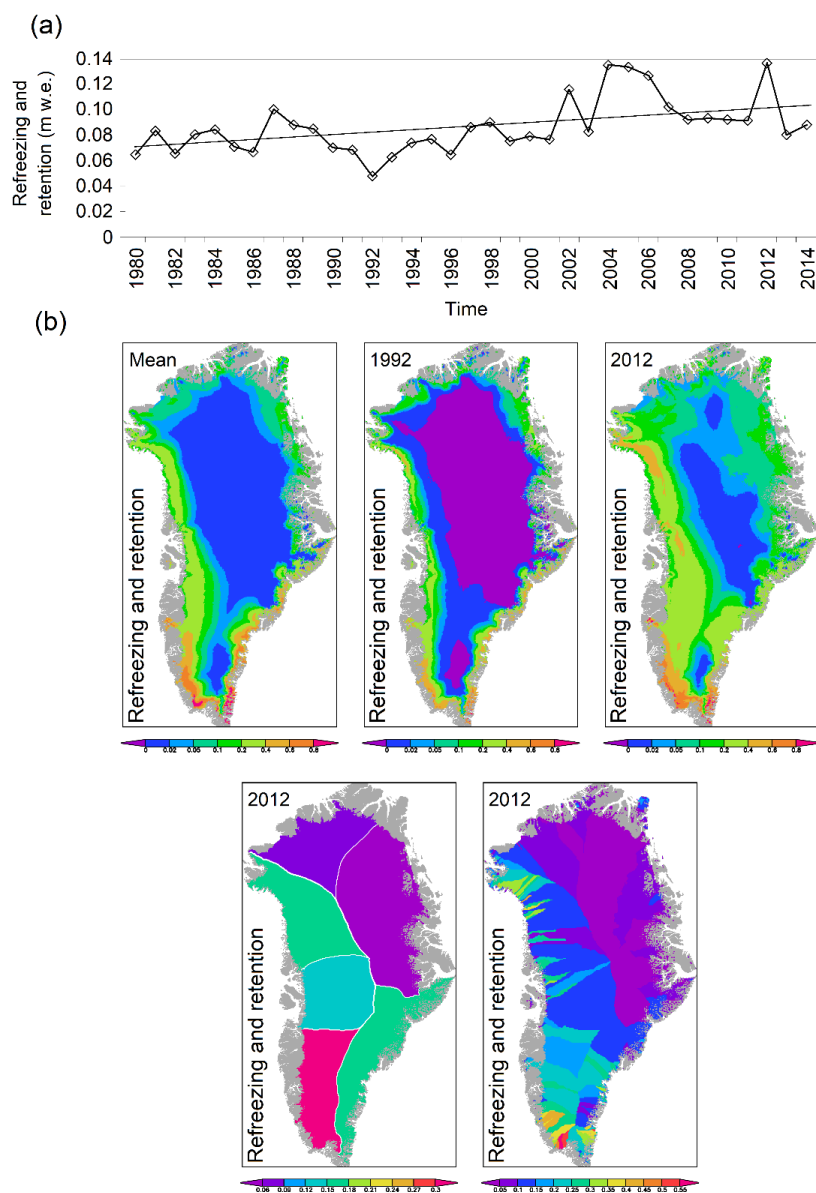
1025

Figure 3: (a) SnowModel ERA-I simulated time series of GrIS mean annual refreezing and
retention (1979–2014) (m w.e.); and (b) spatial 35-year mean GrIS refreezing and retention and
annual values (m w.e) for 1992 and 2012 (upper row), together with the 2012-division into
regions (lower row left) and catchments (lower row right).

42
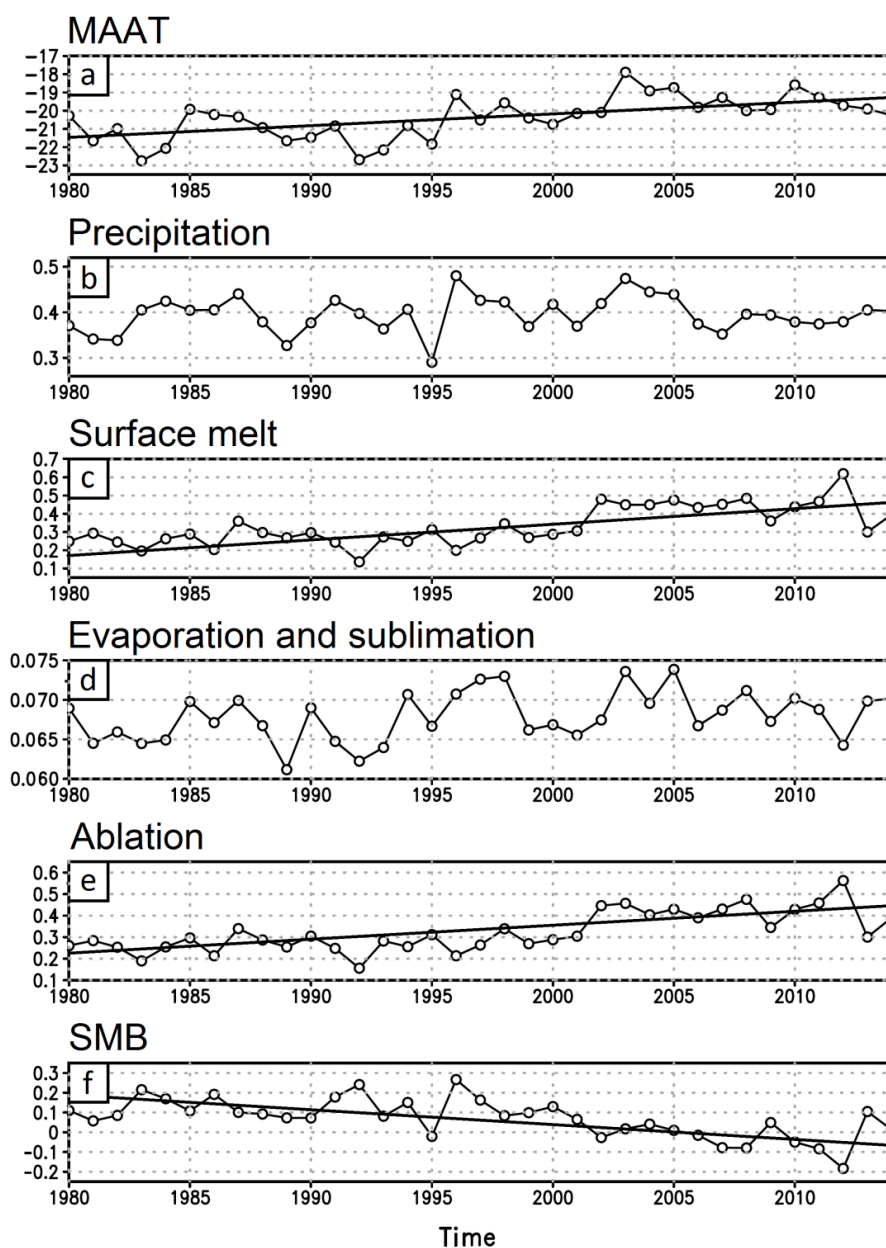
1030

Figure 4: SnowModel ERA-I simulated time series of GrIS annual mean (1979–2014): (a)

MAAT (°C); (b) precipitation (m w.e.); (c) surface melt (snow and ice melt) (m w.e.); (d)

evaporation and sublimation (m w.e.); (e) ablation (m w.e.); and (f) SMB (m w.e.). Only

significant linear trends are shown.
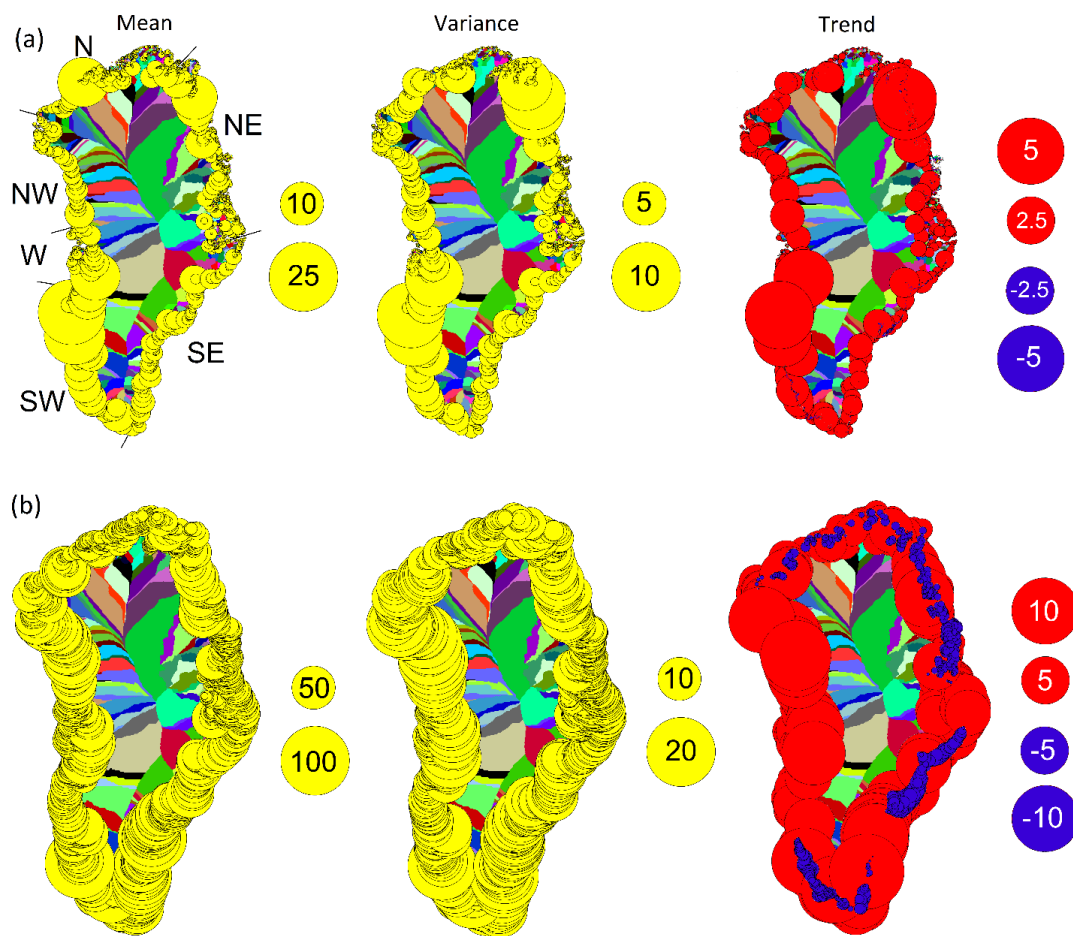
Figure 5: SnowModel ERA-I simulated 35-year spatial Greenland catchment runoff (1979–2014): (a) mean runoff ($\times 10^9$ m^3) (the locations of the major regions SW, W, NW, etc., are illustrated), runoff variance (here illustrated as one standard deviation; $\times 10^9$ m^3), and decadal runoff trends (linear; $\times 10^9$ m^3 decade^{-1}) (catchments with increasing runoff trends are shown with red and decreasing trends with blue colors); and (b) mean specific runoff (L s^{-1} km^{-2}), specific runoff variance (L s^{-1} km^{-2}), and specific runoff trends (linear; L s^{-1} km^{-2} decade^{-1}).
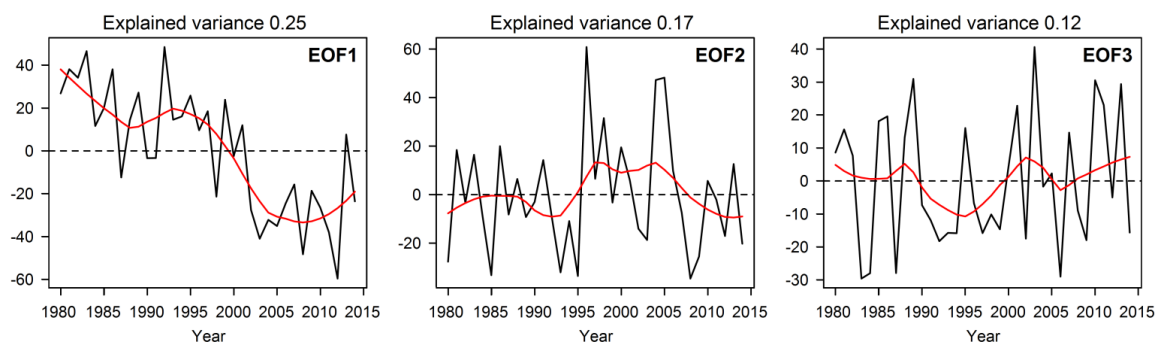
Figure 6: SnowModel ERA-I simulated runoff time series (1979–2014) of the empirical

orthogonal functions (black curve) and 5-year running mean smoothing line (red curve) of EOF1,

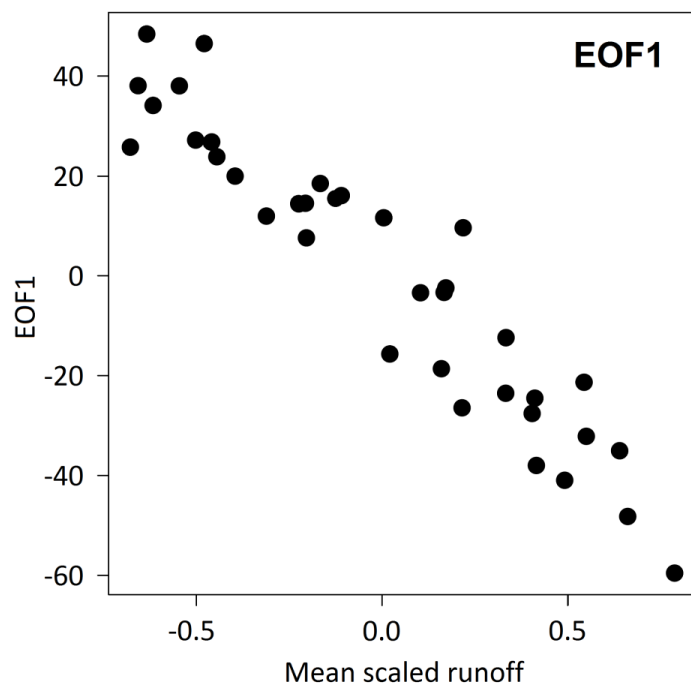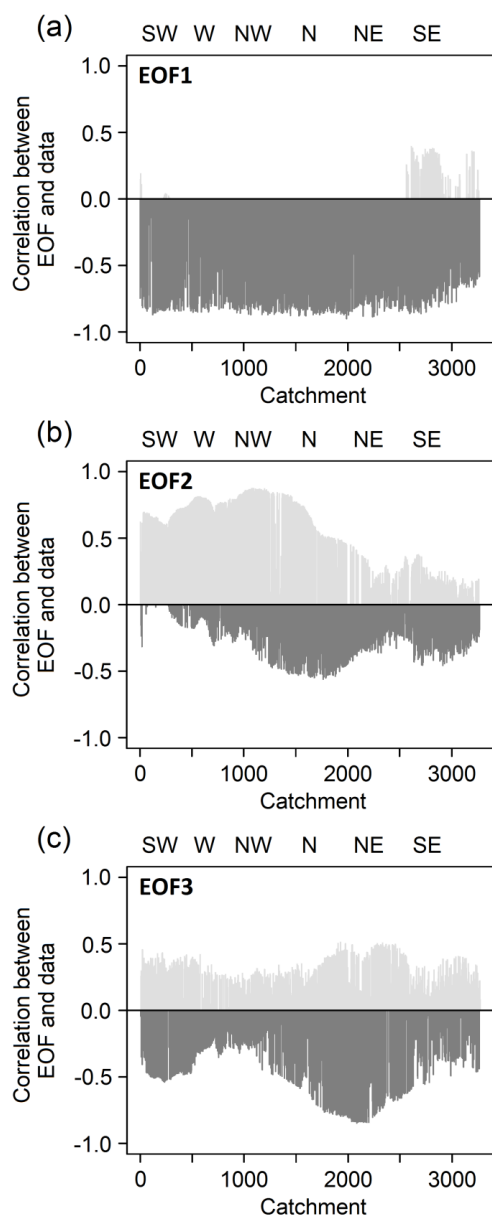EOF2, and EOF3. The explained variance is shown for each EOF, where only EOF1 is

significant.

1068
1069   **Figure 7:** EOF1 cross correlation relationships with mean annual scaled runoff from Greenland.

1070

Figure 8: Eigenvector correlation values for each simulated catchment (1 to 3,272) for: (a)

EOF1; (b) EOF2; and (c) EOF3. From left to right on the lower x-axis the catchments follows the

clockwise path from the southern tip of Greenland (Southwest Greenland, Catchment 1) to the

northern part (N section) and back to the southern tip (Southeast Greenland, Catchment 3,272).

The location of the major regions: SW, W, NW, etc., are shown on the upper x-axis.
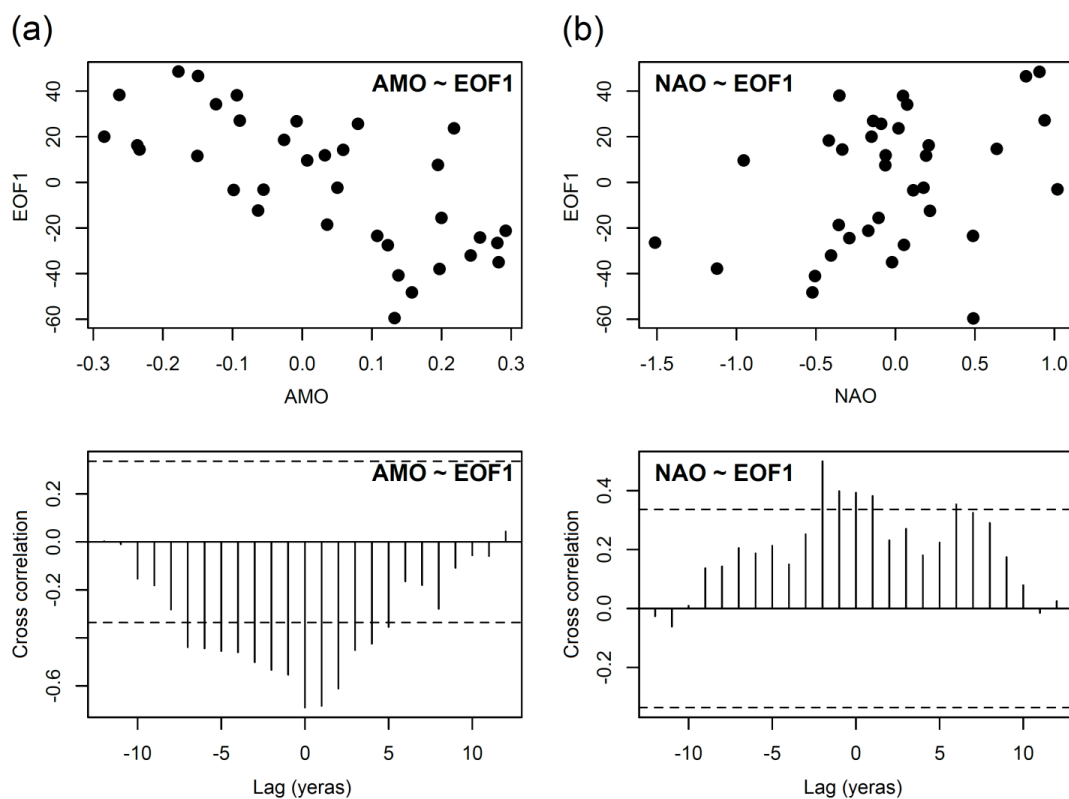
47

Figure 9: EOF1 cross correlation relationships between simulated Greenland runoff: (a) AMO and (b) NAO. The horizontal dashed lines on each of the column charts indicate the significance (95% confidence).

1088 **Table 1:** Regional breakdown of GrIS surface mean annual conditions (units are in Gt) and
1089 trends (linear; Gt decade^{-1}): precipitation (P) (including rain and snow), surface melt, evaporation
1090 (E) and sublimation (Su), runoff (R), ablation, refreezing and retention, and surface mass-balance
1091 (SMB) for GrIS and for each of the six regions both from 1979–2014 (35 years) and 2005–2014
1092 (10 years). Specifically for rain the %-value of total precipitation is shown. Trends are shown in
1093 paragraphs for the GrIS column. Significant trends ($p < 0.05$) are highlighted in bold.

	N (229,075 km^2)	NE (454,900 km^2)	SE (250,425 km^2)	SW (213,550 km^2)	W (231,150 km^2)	NW (267,075 km^2)	GrIS (1,646,175 km^2)
				1979–2014			
P	31.1 ± 5.4	68.4 ± 10.6	242.6 ± 39.1	142.3 ± 23.3	85.4 ± 13.5	84.2 ± 13.9	653.9 ± 66.4 (9.0)
P (rain)	0.4 ± 0.2 (1 %)	0.4 ± 0.2 (<1 %)	4.2 ± 1.8 (2 %)	6.6 ± 2.8 (5 %)	1.7 ± 0.8 (2 %)	2.2 ± 1.1 (3 %)	15.3 ± 5.4 (2 %) (**3.0**)
P (snow)	30.7 ± 5.3	68.0 ± 10.5	238.5 ± 38.7	135.7 ± 22.7	83.7 ± 13.2	82.0 ± 13.5	638.6 ± 65.0 (6.0)
Surface melt	57.2 ± 24.1	72.2 ± 33.8	101.0 ± 27.1	155.2 ± 48.4	67.4 ± 24.0	89.8 ± 33.2	542.9 ± 175.3 (**121.7**)
E + Su	15.7 ± 0.9	25.3 ± 1.6	16.8 ± 0.8	20.3 ± 1.7	16.4 ± 1.1	17.7 ± 0.9	112.2 ± 5.2 (1.8)
R	50.0 ± 22.7	62.6 ± 31.5	69.2 ± 21.0	112.6 ± 41.8	53.6 ± 19.4	70.0 ± 28.1	418.1 ± 151.1 (**106.4**)
Ablation (E + Su + R)	65.7 ± 22.6	87.9 ± 31.5	86.0 ± 21.4	132.9 ± 42.2	70.0 ± 19.9	87.7 ± 28.5	530.3 ± 153.0 (**108.2**)
Refreezing and retention (rain and surface melt minus runoff)	7.6 ± 2.8 (13 %)	10.0 ± 4.0 (14 %)	36.0 ± 8.9 (30 %)	49.2 ± 13.3 (30 %)	15.5 ± 6.1 (22 %)	22.0 ± 7.2 (24 %)	140.1 ± 35.5 (25 %) (**18.3**)
SMB	-34.6 ± 24.8	-19.6 ± 32.4	156.6 ± 44.5	9.3 ± 50.3	15.4 ± 23.6	-3.5 ± 32.1	123.7 ± 163.2 (**-99.2**)
				2005–2014			
P	30.9 ± 5.1	71.0 ± 11.9	232.4 ± 25.2	138.5 ± 16.1	86.4 ± 8.6	85.3 ± 16.9	645.0 ± 39.0 (-5.1)
P (rain)	0.5 ± 0.3 (2 %)	0.4 ± 0.2 (<1 %)	5.2 ± 1.9 (2 %)	7.8 ± 2.3 (6 %)	2.0 ± 0.6 (2 %)	2.9 ± 1.3 (4 %)	18.7 ± 3.4 (3 %) (-2.8)
P (snow)	30.4 ± 5.0	70.6 ± 11.9	227.1 ± 25.0	130.8 ± 15.7	84.4 ± 8.6	82.9 ± 16.4	626.3 ± 39.2 (-2.3)
Surface melt	75.9 ± 26.9	101.7 ± 34.5	129.7 ± 16.3	202.4 ± 39.2	89.3 ± 19.7	124.6 ± 26.8	713.4 ± 138.6 (-79.7)
E + Su	15.7 ± 1.0	25.9 ± 1.1	17.3 ± 0.9	20.7 ± 1.5	16.7 ± 0.8	17.8 ± 0.9	114.1 ± 4.3 (-3.8)
R	67.6 ± 25.0	89.3 ± 31.0	91.7 ± 14.4	154.4 ± 36.3	71.2 ± 15.2	99.5 ± 22.4	573.7 ± 119.8 (-26.0)
Ablation (E + Su + R)	83.3 ± 24.7	115.2 ± 30.8	109.0 ± 14.2	175.1 ± 35.2	87.9 ± 15.0	117.3 ± 22.5	687.8 ± 118.8 (-29.8)
Refreezing and retention (rain and surface melt minus runoff)	8.8 ± 3.5 (12 %)	12.8 ± 5.3 (13 %)	43.3 ± 6.9 (32 %)	55.8 ± 12.1 (27 %)	20.1 ± 6.0 (22 %)	28.0 ± 8.1 (22 %)	158.4 ± 34.4 (22 %) (-56.6)
SMB	-52.4 ± 26.3	-44.2 ± 30.6	123.4 ± 35.7	-36.6 ± 45.0	-1.5 ± 16.4	-31.5 ± 29.7	-42.9 ± 133.5 (24.7)

1094   **Table 2:** Regional breakdown of GrIS specific runoff (L s^{-1} km^{-2}) and changes in specific runoff

1095   (linear; L s^{-1} km^{-2} decade^{-1}) for GrIS and each of the six individual sections both from 1979–

1096   2014 and 2005–2014. Changes in specific runoff are shown in the brackets.

1097

	N	NE	SE	SW	W	NW	GrIS
1979–2014	6.9 (1.6)	4.4 (1.5)	8.8 (1.9)	16.7 (4.1)	7.4 (1.8)	8.3 (2.1)	8.1 (2.0)
2005–2014	9.4 (-0.5)	6.2 (-1.0)	11.6 (-0.1)	22.9 (0.7)	9.8 (-0.5)	11.8 (1.5)	11.1 (-1.3)

1098